STRUCTURAL CONTROL AND HEALTH MONITORING
Struct. Control Health Monit. 2004; **11**:189–221 (DOI: 10.1002/stc.36)

Testing and modelling a semi-actively controlled steel frame structure equipped with MR dampers

Emanuele Renzi[1] and Giorgio Serino[2,*,†]

[1] *ENEA MAT-QUAL, C.R. Casaccia, V. Anguillarese 301, 00060 S. Maria di Galeria, Roma, Italy*
[2] *Department of Structural Analysis and Design, University of Napoli 'Federico II', Via Claudio 21, 80125 Napoli, Italy*

SUMMARY

In this paper, analysis of the shaking table tests performed on a four storey, large-scale, steel mock-up, equipped with a bracing system including magnetorheological (MR) dampers operating both in passive and semi-active (SA) ON–OFF mode, is presented. The adopted SA control algorithm is derived from an 'energy-based' instantaneous optimal control process.

After having described the testing set-up and the control algorithm, a critical overview of the experimental results is reported. In particular, by using SA-controlled MR dampers, large response reductions, with respect to the corresponding passive (ON state) control configuration, may be obtained both in terms of relative displacements (drifts) and absolute accelerations. Moreover, it is experimentally confirmed that use of SA control, not only reduces the maximum values of the considered response quantities, but extends the improvements to the complete time-histories. This satisfactory performance is obtained, even if some particular (and undesired) types of behaviour, shown and explained in the paper, have been detected during the test campaign.

In order to completely understand the dynamical behaviour of the controlled structure and to predict its response, a detailed analytical model of the controlled mock-up is proposed and validated. Copyright © 2004 John Wiley & Sons, Ltd.

KEY WORDS: semi-active control; MR dampers; shaking table tests; energy-based algorithm; instantaneous optimal control; controlled structure modelling

1. INTRODUCTION

In the field of structural control, semi-active (SA) control techniques represent a promising technological evolution of passive control, especially for civil engineering applications. The principal characteristic of SA systems is that control forces are not realized, as in the active case, by using externally positioned actuators (which in civil applications require large power supply), but by modifying, in real-time and according to a preselected control algorithm, the mechanical characteristics of special devices (SA links), that interact (through internal 'reactive' control

*Correspondence to: Giorgio Serino, Department of Structural Analysis and Design, University of Napoli 'Federico II', Via Claudio 21, 80125 Napoli, Italy.
† E-mail: serino@unina.it

Contract/grant sponsor: European commission; contract/grant number: EVG1-CT-1999-00016

Received 28 May 2003
Revised 8 October 2003
Accepted 29 October 2003

Published online 8 June 2004

forces) with the structure. The energy required for the modification of the mechanical parameters of the devices is minimal, and may be furnished even by a simple battery. The regulation modalities of the device parameters are determined, following the selected control algorithms, as a function of the measures of the excitation and/or of the structural response, which implies use of sensors, processors and actuators (to modify the SA links), as is typical of active control.

The SA links, which connect different structural parts, can show a substantially viscous behaviour, e.g. by using variable-orifice hydraulic dampers, plastic behaviour, by using variable friction devices, or visco-plastic behaviour, by using controllable fluids (magnetorheological MR or electrorheological ER); a state-of-the-art review of SA devices may be found in the literature [1].

1.1. Literature overview on dynamical experiments on SA-controlled structures

The first ideas on SA control go back to Karnopp *et al.* [2] in the field of automotive suspensions, but the first application to civil engineering was proposed by Hrovat *et al.* in 1983 [3]. Since these pioneering approaches, many studies have been presented on SA control; a large part of them are concerned with analytical, theoretical and design aspects [4], many others focus on proposals of SA devices (design, manufacturing and testing) [1], but only a minor number of works deal with large-scale dynamical experiments (e.g. with shaking tables) or full-scale applications of these systems.

Probably one of the first shaking table experimentation on SA controlled systems was performed on a three-storey steel model equipped with an active variable stiffness (AVS) system designed by Kajima Corporation and operated at 30 W power [5].

SA variable-orifice fluid viscous dampers (maximum force 8.9 kN, average requested power 55 W) [6] have been tested at SUNY Buffalo on a 1:4-scale three-storey steel frame (mass 3 tons), showing that there are practically no improvements with respect to the same passively operating devices; the same SA variable-orifice fluid viscous dampers have also been tested in a hybrid isolation system [7].

Again at SUNY Buffalo, three separate structures have been tested with hydraulic SA devices (called operational switches) [8]; the first structure was a small-scale metal frame (mass 250 kg), the second was a three-storey frame and the third a four-storey moment-resistant steel frame (mass 3.3 tons).

Very small mock-ups have been used for testing a few MR devices: a MR damper has been installed on a 1:10-scale three-storey steel frame model (mass 227 kg) and tested at University of Notre Dame [9]; Yi *et al.* [10] report dynamical tests on a six-storey (single-bay) steel frame (mass 147 kg), controlled by two shear mode MR dampers, performed at Washington University; whereas Ruangrassamee and Kawashima [11] report the dynamic characterization of a MR damper and shaking table tests on a steel bridge model (mass 370 kg). More recently [12] shaking table tests (executed at NCREE, Taiwan) on a single-storey steel building (mass 1.98 tons) controlled by two MR dampers (maximum force 1 kN) are reported.

However, not so many testing campaigns involving SA control have been realized on large-scale models. One of these examines shaking table tests (performed at ENEL.Hydro–ISMES, Bergamo, Italy) on a one-storey four-column steel frame (mass 8.5 tons) equipped with semi-active oleodynamic devices [13]. Finally, three *in situ* applications of SA-controlled structures can be found in the literature. The first [14], deals with a three-storey building built in 1990 and

equipped with the above mentioned active variable stiffness (AVS) SA devices, by Kajima Corporation; the second [15], describes the first non-passive *in situ* application of structural control in USA, in which controllable fluid viscous dampers were installed, in 1997, on a highway bridge (Walnut Creek Bridge, Highway I-35, OK); and the third [16], describes a five-storey building, built in 1998, again by Kajima Corporation, at Shizouka, where eight controllable viscous dampers were installed. Finally, a new application for SA control of a base isolated building, again in Japan, has been announced [17].

1.2. Introduction to the present experiments

Within the SPACE (Semi-active and PAssive Control of the Dynamic Behaviour of structures subjected to Earthquakes, wind and vibrations) research project founded by European Commission (5th FP, 1998–2002), a shaking table experimental campaign has been performed on a large-scale steel structural mock-up, equipped with a passive and semi-active control system, based on the use of the magnetorheological dampers manufactured within the same project and installed in special bracings.

In the following, after having described the experimental set-up and the control system and deriving a physically meaningful control algorithm, a critical review of the results obtained is reported. The analysis of the experimental evidence allows the formulation of a mathematical model of the passively and semi-actively controlled structure. This mathematical model, of large importance for a complete understanding of the dynamical behaviour of the controlled structure and for predicting its response, is finally illustrated.

2. THE EXPERIMENTAL SET-UP

The experimental campaign, whose results are analysed in this paper, has been carried out on a large-scale steel structural model (called MISS), equipped with a control system consisting of four bracings, each composed of an elastic steel column connected to the main structure through an MR damper which may operate in passive or semi-active mode.

2.1. The MISS structure

MISS (Figure 1) is a 4-storey steel structure owned by ENEA and composed of six vertical columns (HEB100) 4.5 m high, supporting four horizontal frames (3.3×2.1 m in plan) with an inter-storey height of 0.9 m; of the three transversal plane frames, the two external ones are called frame A and B. The columns support four floor slabs manufactured again from HEB100 beam elements, each supporting four concrete blocks. The total mass of the structural mock-up is about 23 tons. As shown in Figure 1, the two lower bracings are positioned between the ground and second floors, the upper ones between the second and fourth floors.

2.2. The semi-active bracings

Various previous studies [4, 18] have shown that, generally speaking, for a passive or semi-active bracing system installed on a framed structure, the optimal value of the stiffness of the bracings is of the same order of magnitude as that of the frame; moreover, in multi-storey frames, the optimal distribution of the bracing stiffnesses decreases linearly with height [19].

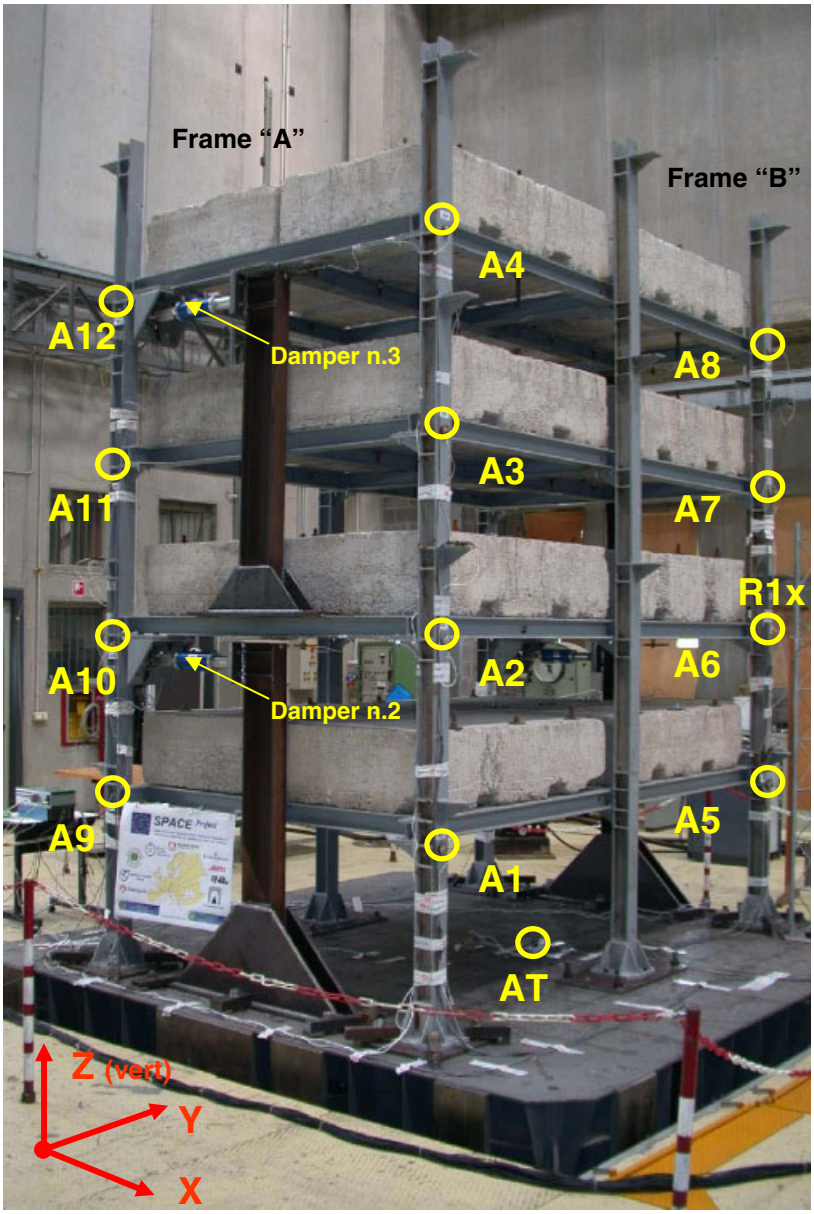

Figure 1. View of MISS on the shaking table with flexible braces and MR devices.

Taking this into account, IPE200 profiles have been selected for the elastic braces. In order to obtain the desired distribution of bracing stiffness, the free length of the braces was reduced by means of reinforcing plates at the base.

A MR fluid contains small metal particles that can be orientated in response to an externally applied magnetic field; by controlling this magnetic field the rheological properties of the fluid

may be regulated, changing from viscous liquid to semi-solid with controllable yield strength [1]. A MR damper is an hydraulic damper filled with a MR fluid; these dampers do not contain moving parts, other than the piston, and therefore appear very reliable in comparison with other SA control devices, which involve electrically controlled valves or mechanisms.

The overall dimensions of each MR device (Figure 2) are $712 \times 200 \times 250$ mm and its mass, without connections, is approximately 20 kg; the device can carry a maximum allowable force of 50 kN along its longitudinal axis and the piston stroke is equal to ± 25 mm. The design procedure used in the determination of the damper mechanical characteristics may be found elsewhere [20].

In the experimental campaign, the shaking table was driven only along the direction of the braced frames (transverse direction, x). Owing to the symmetry of the MISS structure and of the control systems no significant torsional response was observed during the tests.

2.3. *Preliminary tests on the MR dampers*

Preliminarily to the shaking table tests, the MR dampers have been subjected to a wide range of experimentation, in order to verify the actual mechanical properties of the passively operating MR dampers and to obtain information regarding their response times in active operation [21].

The interpretation of these tests has shown the limits of the classical linear Bingham model in the interpretation of the actual dynamical behaviour of these prototype MR dampers, for different driving current i and test frequency. In particular, in order to take correct account of the frequency dependence of the model mechanical parameters, a nonlinear relationship between viscous damping force and velocity was derived:

$$F_{\mathrm{d}}(U, i) = c_{\mathrm{d}}(i)|U|^{\alpha(i)} \operatorname{sgn}(U) + f_{\mathrm{y}}(i) \operatorname{sgn}(U) \tag{1}$$

where F_{d} is the total force in the damper, U the relative velocity across the damper, c_{d} the viscous coefficient and f_{y} the frictional component in the Bingham model. The tests on

Figure 2. MR damper and detail of connection to the structure.

the devices indicated that f_y and c_d may be assumed linearly variable with the current i (expressed in A):

$$c_d(i) = 5.5 + 5.0\,i \text{ (kN (s/m)}^{\alpha}) \qquad f_y(i) = 0.9 + 9.6\,i \text{ (kN)} \tag{2, 3}$$

while the power α can be considered as a quadratic function:

$$\alpha(i) = 0.0795\,i^2 - 0.3475\,i + 0.9 \tag{4}$$

Considering the operational range of the current in passively and ON–OFF semi-actively controlled shaking table tests studied in this paper, i.e. $i = 0$ A and $i = 2.5$ A, the parameters that characterize the constitutive law in Equation (1) are:

$$i = 0 \text{ A} \quad \text{Device OFF}: \quad f_y = 0.9 \text{ kN} \quad \alpha = 0.90 \quad c_d = 5.5 \text{ kN (s/m)}^{0.90} \tag{5a}$$

$$i = 2.5 \text{ A} \quad \text{Device ON}: \quad f_y = 24.5 \text{ kN} \quad \alpha = 0.53 \quad c_d = 18.0 \text{ kN (s/m)}^{0.53} \tag{5b}$$

During these tests on the devices, it has been shown that the operational delays of the SA MR dampers, from the time instant at which the control algorithm changes the command signal to the instant at which the mechanical properties of the MR damper start to be modified, are quite independent of the test frequency and are of about 10 ms both in ON–OFF and OFF–ON phases [21]. The time in which the mechanical parameters, starting from their initial values, reach their final values (e.g. for f_y in the ON–OFF phase, from 24.9 to 0.9 kN), conventionally defined as the time in which 90% of the force variation is completed, is certainly dependent on the damper scale and it has been evaluated as about 20 ms in the ON–OFF case and 30 ms in the OFF–ON phase.

3. CONTROL ALGORITHM

For a n-degrees-of-freedom controlled linear system subjected to base acceleration, the equations of motion can be expressed in the state-space as follows:

$$\dot{\boldsymbol{z}}(t) = \boldsymbol{A}\boldsymbol{z}(t) + \boldsymbol{B}\boldsymbol{f}(t) + \boldsymbol{e}w(t) \tag{6}$$

where $\boldsymbol{z}$ is the (relative, with respect to the ground) state vector, $\boldsymbol{f}$ is the vector of the control forces (generated in the p control devices) and w is the base acceleration. In general, the system matrices have the following, well-known, form

$$\boldsymbol{z}(t) = \begin{bmatrix} \boldsymbol{x}(t)_{n,1} \\ \dot{\boldsymbol{x}}(t)_{n,1} \end{bmatrix}_{2n,1} \qquad \boldsymbol{A} = \begin{bmatrix} \boldsymbol{O}_{n,n} & \boldsymbol{I}_{n,n} \\ -\boldsymbol{M}^{-1}\boldsymbol{K} & -\boldsymbol{M}^{-1}\boldsymbol{C} \end{bmatrix}_{2n,2n} \tag{7a, b}$$

$$\boldsymbol{B} = \begin{bmatrix} \boldsymbol{O}_{n,p} \\ \boldsymbol{M}^{-1}\boldsymbol{L} \end{bmatrix}_{2n,p} \qquad \boldsymbol{e} = \begin{bmatrix} \boldsymbol{O}_{n,1} \\ -\boldsymbol{I}_{n,1} \end{bmatrix}_{2n,1} \tag{7c, d}$$

where $\boldsymbol{x}$ is the displacement vector, $\boldsymbol{M}$, $\boldsymbol{K}$ and $\boldsymbol{C}$, respectively, the mass, stiffness and damping matrices of the non-controlled structure, $\boldsymbol{L}$ the allocation matrix of the control forces, $\boldsymbol{O}$ and $\boldsymbol{I}$ null and identity matrices of appropriate dimensions.

For the derivation of a general ON–OFF control law the following instantaneous performance index (PI) [22], may be introduced:

$$J(\boldsymbol{z}, t) = \tfrac{1}{2}\boldsymbol{z}^{\mathrm{T}}(t)\boldsymbol{Q}\boldsymbol{z}(t) \tag{8}$$

where $\boldsymbol{z}$ is the state vector and $\boldsymbol{Q}$ is a weighting (positive semi-definite) matrix. Since it is not possible to modify the actual value of the PI, the control strategy is based on the selection of the control forces $\boldsymbol{f}(t)$ which guarantee the future value of such a function to be as small as possible. This is obtained by minimizing the contribution that the control forces make to the time derivative of the PI.

Considering Equation (6), the time derivative of the PI has the following form:

$$\dot{J}(t) = \boldsymbol{z}^{\mathrm{T}}(t)\boldsymbol{Q}\dot{\boldsymbol{z}}(t) = \boldsymbol{z}^{\mathrm{T}}\boldsymbol{Q}\boldsymbol{A}\boldsymbol{z} + \boldsymbol{z}^{\mathrm{T}}\boldsymbol{Q}\boldsymbol{e}w + \boldsymbol{z}^{\mathrm{T}}\boldsymbol{Q}\boldsymbol{B}\boldsymbol{f} = \dot{J}^{z}(t) + \dot{J}^{w}(t) + \dot{J}^{f}(t) \tag{9}$$

the only part that may be instantaneously modified by modifying the control forces $\boldsymbol{f}$ is the third part of the sum in Equation (9):

$$\dot{J}^{f}(t) = [\boldsymbol{z}^{\mathrm{T}}(t)\boldsymbol{Q}\boldsymbol{B}]\boldsymbol{f}(t) = \boldsymbol{l}^{\mathrm{T}}(t)\boldsymbol{f}(t) = \sum_{i=1}^{m} l_i(t)f_i(t) \tag{10}$$

Equation (10), which includes the definition of the vector $\boldsymbol{l}(t)$ (dimensions: $p, 1$), is as negative as possible if the single contributions to the sum are negative; in other words the ith semi-active control device is active only if it contributes with a non-positive term to the sum in Equation (10). Therefore, the control algorithm selects the state of the control device, independently of those assumed by the others, in accordance with the following condition:

$$l_i(t)f_i(t) \leqslant 0 \Rightarrow i\text{th element active} \tag{11}$$

Note that, generally speaking, the $\boldsymbol{l}(t)$ vector has the following form:

$$\boldsymbol{l}^{\mathrm{T}} = \boldsymbol{z}^{\mathrm{T}}(t)\boldsymbol{Q}\boldsymbol{B} = [\,\boldsymbol{x}^{\mathrm{T}} \quad \dot{\boldsymbol{x}}^{\mathrm{T}}\,]\begin{bmatrix}\boldsymbol{Q}_{11} & \boldsymbol{Q}_{12}\\ \boldsymbol{Q}_{21} & \boldsymbol{Q}_{22}\end{bmatrix}\begin{bmatrix}\boldsymbol{O}\\ \boldsymbol{M}^{-1}\boldsymbol{L}\end{bmatrix} = (\boldsymbol{x}^{\mathrm{T}}\boldsymbol{Q}_{12} + \dot{\boldsymbol{x}}^{\mathrm{T}}\boldsymbol{Q}_{22})\boldsymbol{M}^{-1}\boldsymbol{L} \tag{12}$$

The general algorithm (Equation (11)) has the following interesting properties:

P1. Elements $\boldsymbol{Q}_{11}$ and $\boldsymbol{Q}_{21}$ of the weighting matrix $\boldsymbol{Q}$ have no influence on the control algorithm, in fact do not appear in Equations (11) and (12);
P2. The measure of base excitation is not required;
P3. The algorithm appears robust with respect to small measure or modelling errors, in fact only the sign of Equation (11) has to be evaluated;
P4. It may be shown that, if the non-controlled system is stable *per se* and if $\boldsymbol{Q}$ is positive definite, also the controlled system is stable (Lyapounov).

It has been shown that the optimal configuration of the algorithms is obtained if $\boldsymbol{Q}_{12} = \boldsymbol{O}$ [4]. In view of a physical interpretation of the control process, the $\boldsymbol{Q}_{22}$ matrix may be written in the following form, where the dimensionless weights q_i $(i = 1 \ldots n)$, collected in the $\boldsymbol{q}$ $(n, 1)$ vector, are introduced:

$$\boldsymbol{Q}_{22} = [\mathrm{diag}_n(\boldsymbol{q})]\boldsymbol{M} \tag{13}$$

For this position the PI assumes the physical meaning of 'weighted' kinetic energy:

$$J(\boldsymbol{z}, t) = \frac{1}{2}\boldsymbol{z}^{\mathrm{T}}(t)\boldsymbol{Q}\boldsymbol{z}(t) = \frac{1}{2}\dot{\boldsymbol{x}}^{\mathrm{T}}(t)[\mathrm{diag}_n(\boldsymbol{q})]\boldsymbol{M}\dot{\boldsymbol{x}}(t) = \frac{1}{2}\sum_{i=1}^{n} q_i m_i \dot{x}_i^2(t) \tag{14}$$

consequently the $\boldsymbol{l}(t)$ vector (Equation (12)) assumes the following (simple) form:

$$\boldsymbol{l}^{\mathrm{T}}(t) = \dot{\boldsymbol{x}}^{\mathrm{T}}(t)[\mathrm{diag}_n(\boldsymbol{q})]\boldsymbol{L} \tag{15}$$

In this case the algorithm shows the following additional properties, which make the control implementation simple and reliable:

P5. Every single device is controlled independently from all the others;
P6. The state of the device depends only on the 'local' responses, measured at the degrees of freedom connected by the device (decentralized or 'local' control);
P7. The identification of the structural parameters are not required; in fact no masses, stiffness or dampings are involved in Equation (15).

A number of different control algorithms may be obtained by using different forms for the dimensionless weighting vector $\boldsymbol{q}$.

In the present experiments, the absence of torsional response allows the plane model in Figure 3 of the controlled MISS structure ($n = 4,\ p = 2$) to be considered valid. If the masses of the bracings vanish with respect to those of MISS, the design simplified model has only four degrees of freedom; in this case, by setting $q_1 = q_2 = q_3 = q_4 = 1$, the control process minimizes the kinetic energy of MISS, Equation (9) represents the instantaneous power balance and the sum in Equation (10), which represents, if positive, the energy flow from the control system to the structure, becomes:

$$\dot{J}^f(t) = \boldsymbol{l}^{\mathrm{T}}(t)\boldsymbol{f}(t) = \dot{x}_2(t)f_1(t) + [\dot{x}_4(t) - \dot{x}_2(t)]f_2(t) \tag{16}$$

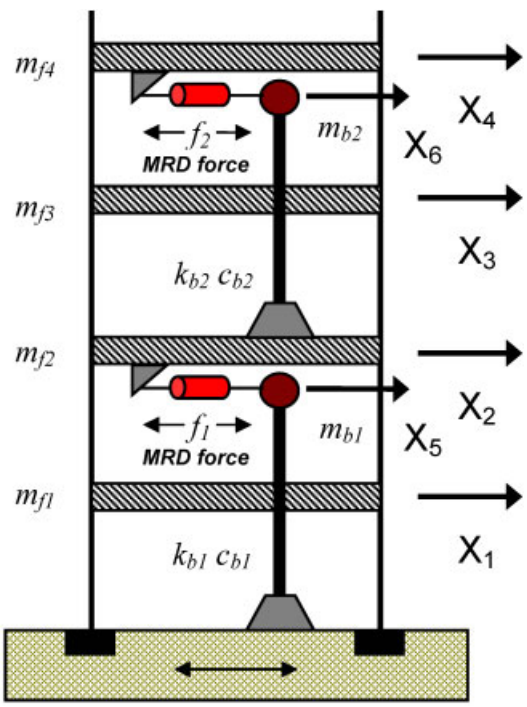

Figure 3. Model of the controlled MISS structure.

For these positions, the control algorithm, which determines the activation of the MR devices, assumes the following form:

$$\text{if } \dot{x}_2(t)f_1(t) < \varepsilon \quad \text{device 1 is active} : u_1(t) = u_{\max} \tag{17a}$$

$$\text{if } [\dot{x}_4(t) - \dot{x}_2(t)]f_2(t) < \varepsilon \quad \text{device 2 is active} : u_2(t) = u_{\max} \tag{17b}$$

where u_1 and u_2 are the currents in the control devices, and ε is a threshold set, in the shaking table tests, to 10^{-3} kN m/s.

It is easy to show that this control law also guarantees the maximum power flow from the main structure (MISS) to the control system (bracings), i.e. the maximum energy dissipation in the control system; for this motivation the algorithm has also been called the 'energy' algorithm.

In practice, following this algorithm, the device is deactivated when the velocity across the bracing reaches (practically) zero, i.e. when the bracing deformation has a relative maximum or minimum, and it is reactivated when the force in the device f_i changes sign. This algorithm practically coincides with that proposed in 1995 by Inaudi and Hayen [23] and also used in other works [18, 19].

4. SHAKING TABLE TESTS

The tests on the MISS mock-up have been performed by using the MASTER (Multi Axes Shaking Table for Earthquake Reproduction) facility available in the Structural Dynamics Testing Laboratory of ENEL.Hydro–ISMES in Seriate (Bergamo, Italy), a six-degrees-of-freedom shaking table of dimensions 4×4 m.

A number of physical quantities have been measured and acquired during the tests, in order to evaluate the structural response, (sensors for the response acquisition):

- the table (AT) and floor accelerations on both sides of MISS (A1–A12, Figure 1);
- the second-floor MISS displacement with respect to the shaking table (R1x, Figure 1), by using a rigid reference structure;
- the voltage input signals commanding the two upper dampers simultaneously (P1) and the two lower ones (P2);
- the currents supplied to the dampers (c1–c4);
- the damper deformations, by measuring the displacement between braces and MISS (LD1–LD4);
- the damper forces, measured by the load cells on the dampers (FD1–FD4).

In order to drive the control system which, in SA-controlled cases, determines the control action depending on the measured responses, the following response quantities have been used (sensors for the control system):

- five accelerometers for the table (ACT) and floor absolute accelerations, x direction (AC1–AC4);
- the LVDT indicating the relative displacements across the dampers (LD1–LD4);
- the load cells to measure MR damper forces (FD1–FD4).

Note that the signals for response acquisition have been treated and acquired independently from those used for the control system. In particular, for the accelerations, a different sets of

accelerometers has been used; moreover, the signals acquired for response acquisition have been low-pass filtered at 60 Hz.

For the tests in semi-active configurations, a specific electronic hardware and software (Figure 4) has been used in order to control the MR dampers. These apparatus consists of three parts: a PC processor (Pentium III, 850 MHz) with an ordinary operating system (Windows NT), able to evolve to a real-time acquisition and processing system through the implementation of the programming language Labview Real-Time [24]; two digital acquisition boards (DAQ boards) with a total of 16 inputs and 4 outputs, 16 bit resolutions and a sampling rate of 333 kHz; the software Labview Real-Time, able to extend the Labview graphical programming to create applications with deterministic, real-time performance. Besides, for the operation of the MR dampers, power supplies have been used, each having two bipolar control channels (voltage and current mode), selectable and individually controllable either from its front panel controls, or by remote signals.

As mentioned above, the shaking table tests were performed only in the x direction. In particular, the following inputs have been used:

- for the characterization tests, sinusoidal single axis sweep tests, in the range 0.5–35 Hz, at very low excitation amplitude (up to 0.01 g peak maximum), sweep rate 1 octave/min, have been performed in non-controlled and passive configurations;
- for the seismic tests, the inputs were a synthetic accelerogram, compatible with European Code EC8 for soft soils (CGS), and two natural accelerograms, the first recorded during the 1976 Friuli, Italy, earthquake (Tolmezzo), and the second recorded during the Northridge, California, earthquake of January 17, 1994 (Northridge).

In Figure 5 the time-histories and the acceleration response spectra (for 5% damping factor) of the non-scaled selected seismic inputs are reported.

The following structural configurations have been tested:

NC : non-controlled (unbraced) configuration, in which MISS has been tested without MR dampers;

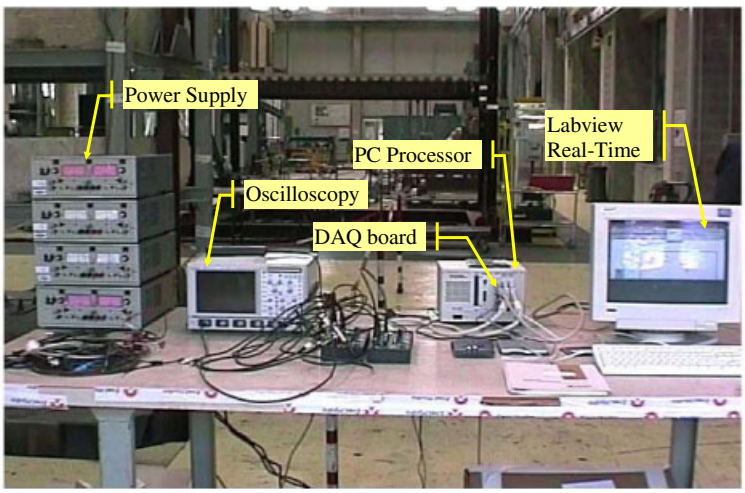

Figure 4. Electronic equipment for semi-active tests.

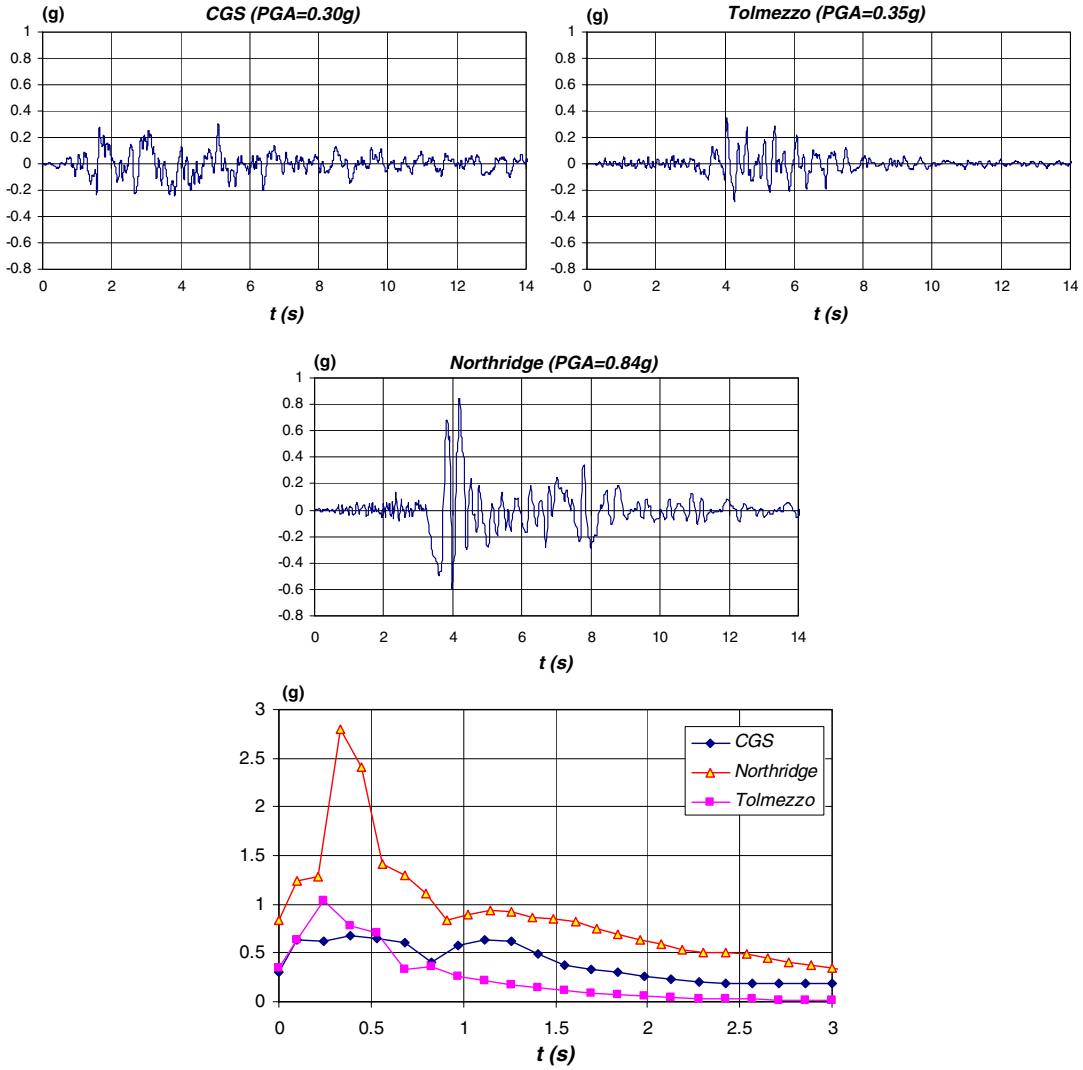

Figure 5. Seismic inputs, unscaled acceleration time-histories and response spectra (5% damping).

PC_0: passive control, 0 A, configuration, in absence of any control signal, i.e. a 0 A current drives the MR devices;

PC_2, 5: passive control, 2.5 A, configuration, in this situation the non-modulated control signal is set to the maximum value, i.e. a 2.5 A constant current drives the MR dampers;

SA_En: semi-active control, 'energy' algorithm, configuration, in this case the control devices are fed with a time-varying input signal according to the ON–OFF algorithm of Equations (17).

In the passive configurations the control system has been fed with a constant control signal (current), and the MR dampers behave as passive devices. This is important also in order to evaluate the control performances in case of wrong operations of the semi-active control system and to give a comparison term for the SA control performances.

In the SA-controlled case the devices in frame A (2 and 3) may be controlled independently from the corresponding ones in frame B (1 and 4), but for practical motivations, during the tests the control of the devices at the same level have been actually driven through a unique control signal.

Typically, for each control configuration, a sweep-sine test has been performed. After it, the seismic tests have been performed at increasing amplitudes, starting from very low amplitude up to the limit value of the second-floor displacement of MISS (20 mm, in order to avoid yielding of the steel columns) or a limit value of the overturning moment of the shaking table (300 kNm).

5. REVIEW AND ANALYSIS OF THE EXPERIMENTAL RESULTS

A large number of tests (over 110) have been performed in the various considered structural configurations.

Concerning the characterization sweep-sine test, performed in the NC, PC_0 and PC_2, 5 control configurations, the most important effect of the bracings, at these low input levels, is the stiffening of the PC_0 and PC_2, 5 structures, the first frequency of which increases up to 3.1 Hz with respect to the 2.2 Hz corresponding value of the NC configuration.

Regarding the seismic tests, it is worth noting that the attainment of higher input levels for a certain configuration is a first immediate index of better performance (see Table I); note that the maximum level reached in semi-actively controlled configurations is 2.5–4 times larger than the maximum level reached in non-controlled configurations.

A more complete comparison of the results, in all the seismic tests, is represented in Figures 6–8, for CGS, Tolmezzo and Northridge inputs, respectively, where, for each seismic input, the peak values of the actually measured table acceleration (ATx), the second- and fourth-floor accelerations (A2x, A4x) and second-floor relative displacement (R1x), are plotted against the corresponding nominal scale factor. Generally speaking, it can be seen that, with respect to the non-controlled (NC) case and for the same scale factor and earthquake input, by using PC operating at 0 A (PC_0) both displacements and accelerations are reduced, whereas, by using PC operating at 2.5 A (PC_2, 5) more important reductions are obtained in terms of

Table I. Maximum nominal scale factors and actual PGA obtained during the seismic tests.

		Control configurations			
Input		NC	PC_0	PC_2,5	SA_En
CGS	Scale factor	0.251	0.631	0.794	1.259
	Actual PGA	0.14 *g*	0.24 *g*	0.34 *g*	0.36 *g*
Tolmezzo	Scale factor	0.251	0.794	1.000	1.000
	Actual PGA	0.19 *g*	0.30 *g*	0.37 *g*	0.44 *g*
Northridge	Scale factor	0.016	0.063	0.126	0.251
	Actual PGA	0.10 *g*	0.21 *g*	0.31 *g*	0.40 *g*

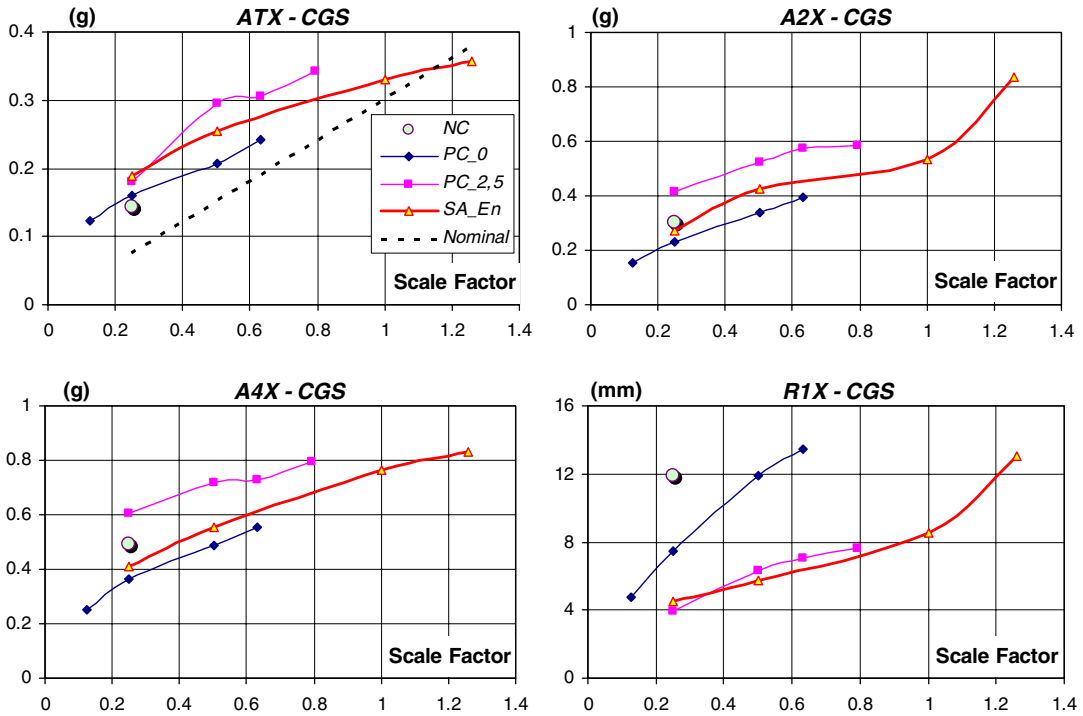

Figure 6. Peak responses as a function of nominal input scale factor in different configurations, CGS.

displacements, but the absolute accelerations result increased with respect to the NC case. Furthermore, by using semi-active control (SA_En) the displacements are further significantly reduced, also with respect to the PC_2, 5 case, whereas the accelerations are not incremented and are included between those of PC_0 and PC_2, 5 cases.

5.1. Passive control (2.5 A current) versus semi-active ON–OFF control

By evaluating the response reductions obtained with the semi-actively controlled MR dampers, the good behaviour of the selected control algorithm has been clearly confirmed. In this subsection a direct comparison between passive controlled, 2.5 A, configuration (PC_2, 5) and semi-actively controlled configuration (SA_En) is reported (Figure 9). Obviously, this direct comparison is possible only if the two configurations have been tested at the same nominal input level, therefore the following considerations apply to: 0.501-scaled CGS, unscaled Tolmezzo and 0.126-scaled Northridge.

By examining these cases it can be seen that large response reductions, with respect to the passive configuration, have been obtained in terms of peak relative structural displacements (second-floor, R1x). These reductions are of about 30–35% for both the natural seismic inputs (Northridge and Tolmezzo), and about 10% for the 'synthetic' seismic input (CGS, Figure 9a). Moreover, in the semi-actively controlled configurations, not only the peak acceleration responses, as mentioned above, are not larger than the ones in the corresponding passive cases

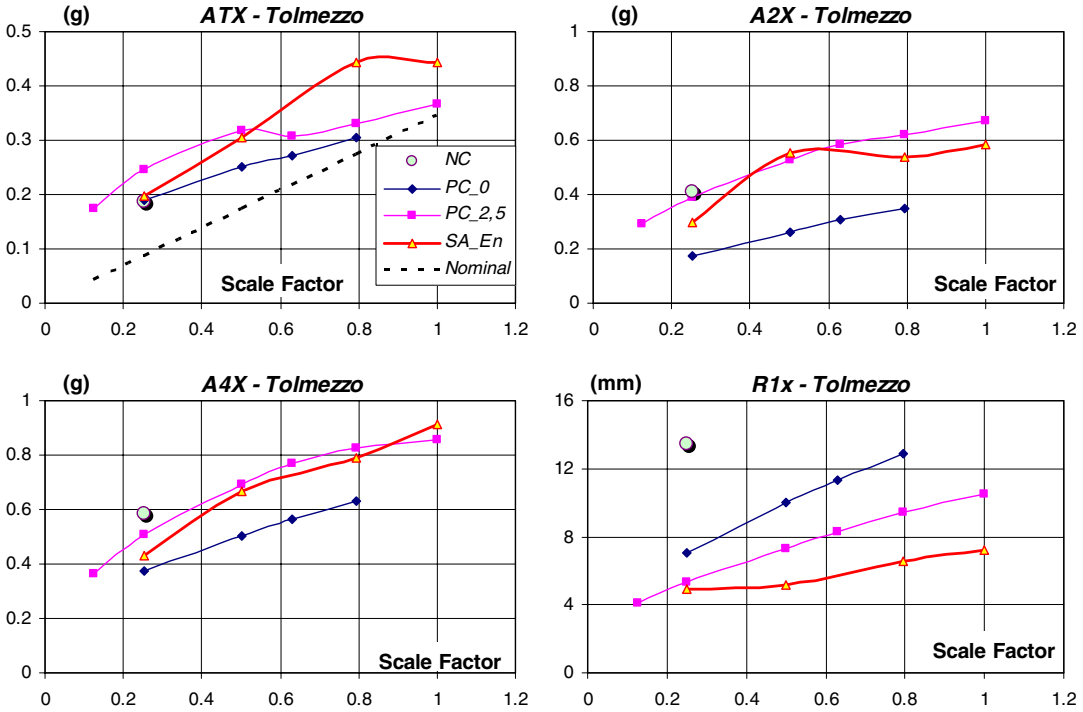

Figure 7. Peak responses as a function of nominal input scale factor in different configurations, Tolmezzo.

(as expected), but in various cases (CGS) also the accelerations are reduced (up to 30%) by the semi-active control (Figure 9b).

It appears, also, that using semi-active control, not only reduces the maximum values of the considered response quantities, but extends the improvements to the complete time-history, see Figures 9(c,d) for the mean responses (rms) over the entire time histories. In particular also the rms accelerations obtained in semi-active cases, in contrast to the peak values, are systematically reduced with respect to the passive control cases, compare Figures 9(b,d). These reduction are quite uniform for both rms displacements and accelerations and are about 15–25% for the three seismic inputs.

The differences between the passive and SA control configurations considered are highlighted, for the Northridge seismic input, in Figure 10, in which the time-histories of the Second-floor relative displacement (R1x) and of the fourth-floor absolute accelerations (A4x), and the force deformation cycles of the MR dampers and of bracing 1 are directly compared. Note the uniform reduction of responses over the entire time-history and the different dissipation mechanism realized in the two cases.

5.2. *Comments on the actual behaviour of the control system*

Important indications of the actual behaviour of the control devices have been obtained by observing force–deformation cycles, such as those of Figure 10:

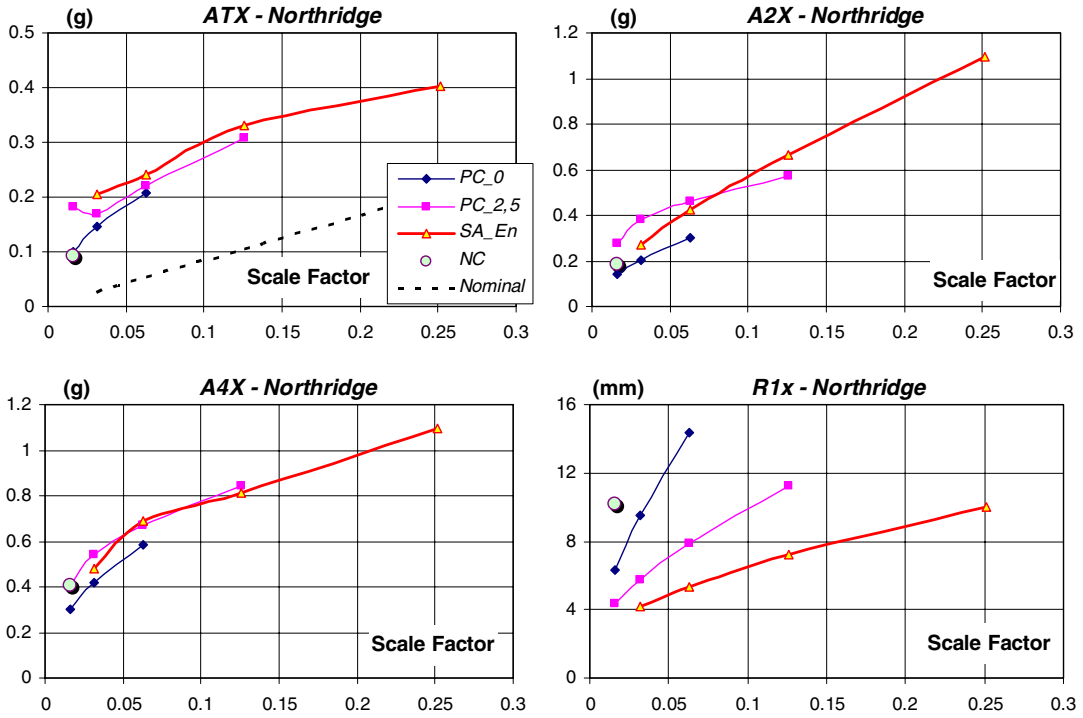

Figure 8. Peak responses as a function of nominal input scale factor in different configurations, Northridge.

- a 'slip' of the damper at zero level force (of roughly 0.85–1.00 mm for damper 1, but even lower for the others), which worsens the control performances in particular in SA cases, has been detected in all the configurations;
- a non-negligible stiffness k_d (approximately constant and equal to 30 kN/mm for each damper) not considered in the Bingham model, is shown in the measured damper response.

It has been observed that these phenomena are not a real response of the damper only, but are due to the connection arrangement between the dampers, the frame and the braces. In the implementation of the 'energy' algorithm, the floor velocities have not been directly measured, but have been evaluated through numerical real-time integration of the floor absolute accelerations.

In Figure 11 an example of the acceleration signals acquired by the control system (AC2) is reported. It can be seen that the floor acceleration signals acquired and processed by the control system show a significant high-frequency component (at about 90 Hz). This high-frequency component is not shown by the sensors for the response evaluation, because these signals have been low-pass filtered ($f_{LP} = 60$ Hz). These disturbances are strictly correlated with the activation of the devices. In fact, it can also be seen, in Figure 11 where the current driving damper 2 (c2) is reported, that the larger signal disturbances (acceleration spikes) correspond to the jumps in the current driving the connected devices, in response to the SA control strategy;

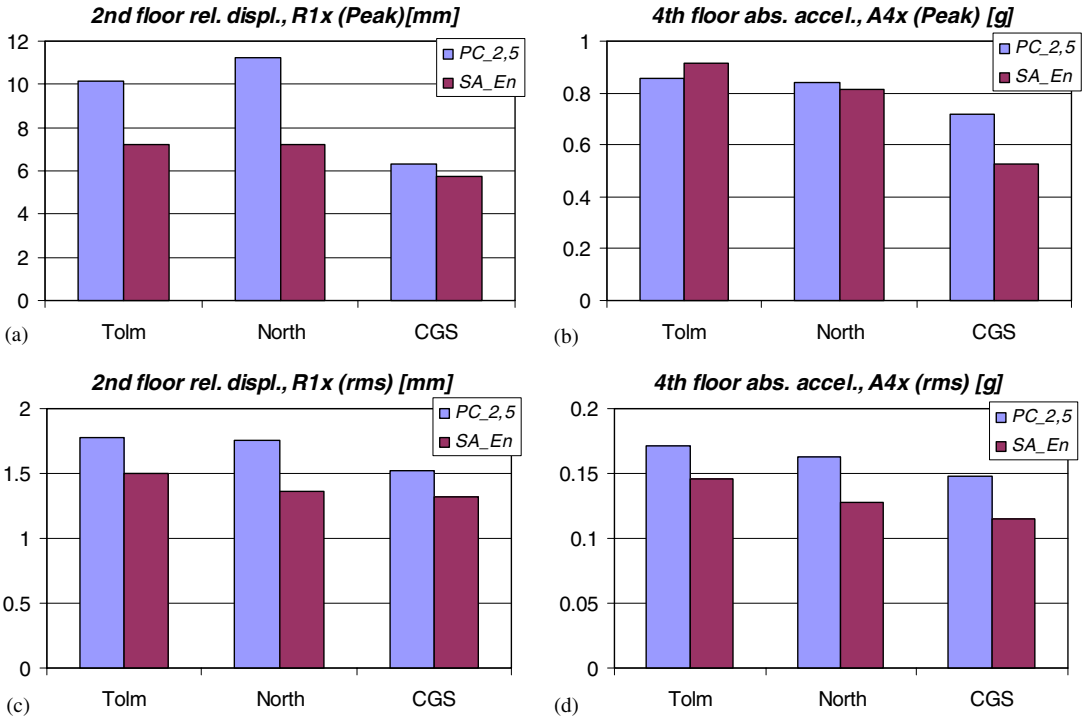

Figure 9. Peak (a, b) and rms (c, d) response in different configurations.

probably, when the reaction force of the MR damper increases quickly, in response to the current signal, a sort of impact, between brace and frame, occurs. This fact confirms that the realization of an ON–OFF semi-active control system may even produce large increments of the floor absolute accelerations, and in particular of their high-frequency components.

Finally, in order to evaluate the effective behaviour of the SA controlled system, in Figure 12, a detail of the response obtained, around the maximum amplitude of Tolmezzo unscaled input, is reported.

In particular, the responses are reported in terms of time-histories (Figures 12a,b) of acquired force in damper 1 (FD1), second-floor velocity (dX2, evaluated by the control system), displacements of damper 1 and of second-floor (LD1, R1x) and current driving damper 1 (c1) and of force–displacement cycles, both for the MR device 1 (Figure 12c) and for the lower brace 1 (Figure 12d). It is useful to observe both the force–displacement cycles, because the first (in which the damper force is reported as a function of damper deformation) shows the behaviour of the MR damper only, but the second (in which the damper force is reported as a function of frame displacement) shows the effective global behaviour of the control system (SA bracing), interacting with the structure to be protected (frame).

The more significant points (or events) of the responses considered, marked in the figure with circles and capital letters, have the following meanings:

A: at this point a relative maximum in the measured second-floor relative displacement (R1x, open circle in Figure 12b) is reached, the sign of the corresponding relative

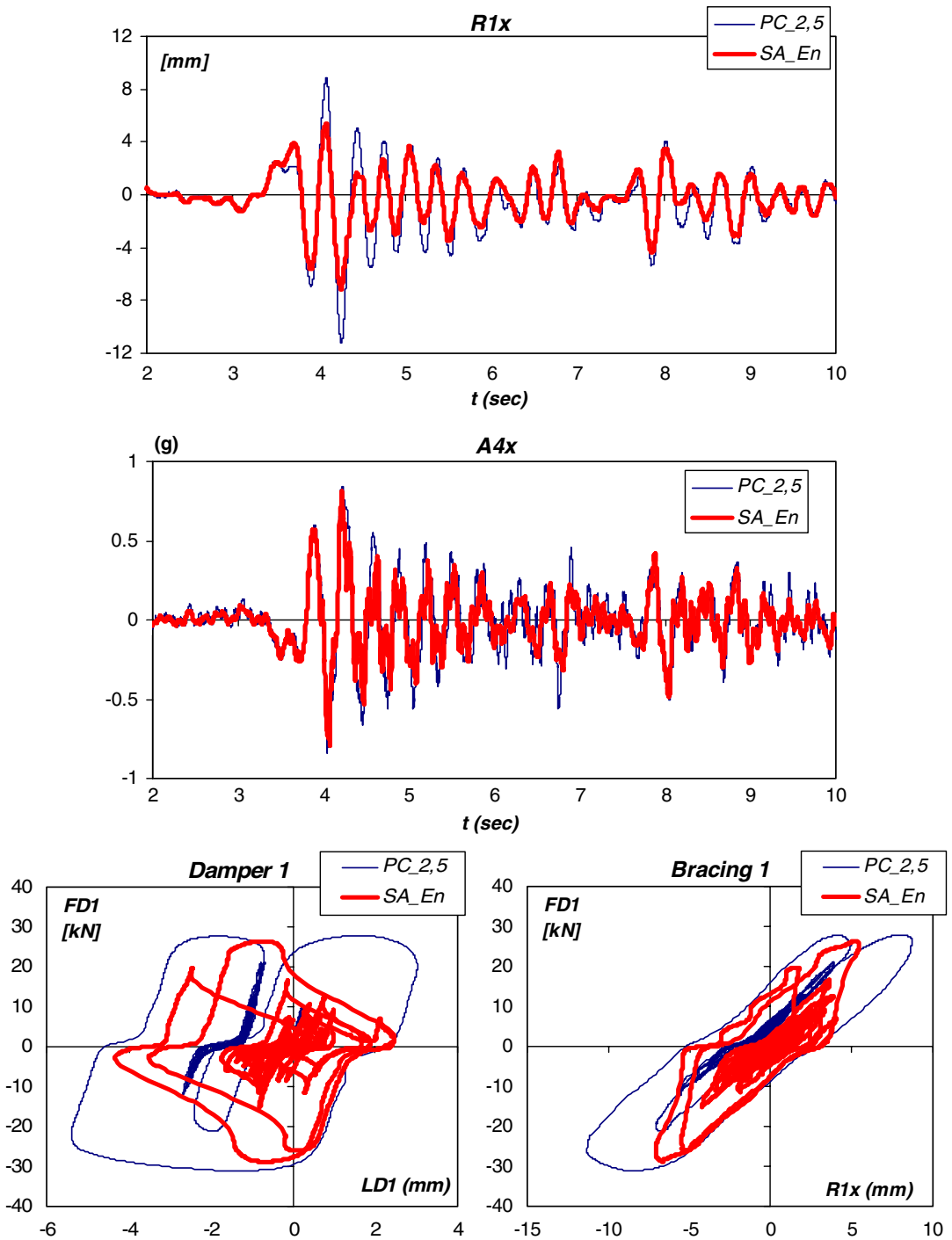

Figure 10. Second-floor displacement, fourth-floor acceleration and hysteretic cycles; Northridge (SF = 0.126).

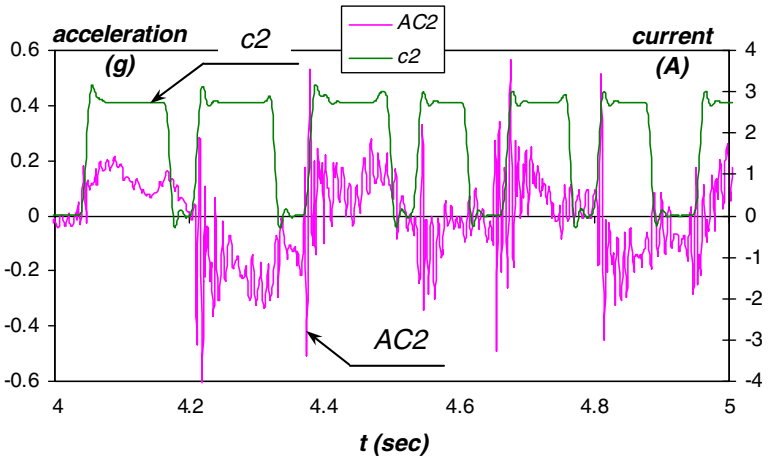

Figure 11. Second-floor acceleration and current driving damper 2. Tolmezzo (SF = 0.251), SA_En.

velocity (dX2, Figure 12a) changes and the device is deactivated; the current driving the MR dampers (c1, Figure 12b) falls, and this causes a sharp change in the force in the device (FD1, Figure 12a);

A–B: the device is not active and its dissipative activity is in progress; the force in the device decreases sharply toward the zero value (FD1, Figure 12a) and a large deformation in the damper occurs (LD1, Figures 12b,c); this happens without significant modification of the frame displacement (R1x, Figures 12b,d). This means that the elastic brace is relaxing very quickly with respect to the frame dynamics, and the stored elastic energy is dissipated by the MR damper in OFF operation;

B: at this time the damper deformation (frame–brace displacement) reaches its maximum (LD1, Figure 12b), the damper starts moving toward its zero-force position, and the force becomes less than the MR frictional force of the damper (in OFF operation, $f_{y,min}$). The dissipation phase has been completed;

B–C: the damper force is less than the frictional component (in OFF state), i.e. the damper is in its 'stick' phase, the damper deformation is little changed (LD1, Figures 12b,c) so that the frame displacement practically corresponds to that in the brace. This means that the frame, inverting its motion direction, starts to drag the brace with itself;

C: at this point the sign of the damper force changes (FD1, Figure 12a) and the control algorithm commands the activation of the device, therefore the sharp increment of the current (c1, Figure 12c) driving the MR damper begins. This time instant should be the beginning of the elastic energy accumulation in the brace;

C–D: the damper is in its ON operation but, due to the slipping of the device already shown, there is a significant damper deformation (slip) at very low force level (Figure 12c) and also the frame, continuing its motion, practically undisturbed shows a large displacement (Figure 12d). This behaviour reduces the elastic energy that can be stored in the brace and to be dissipated at the next deactivation;

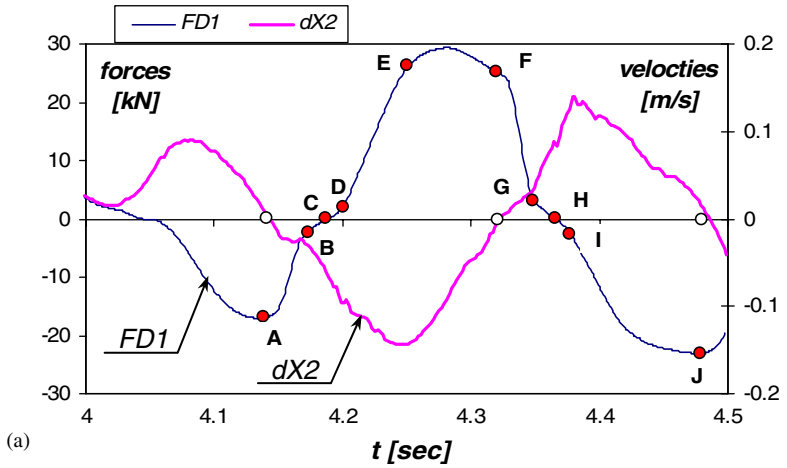

(a)

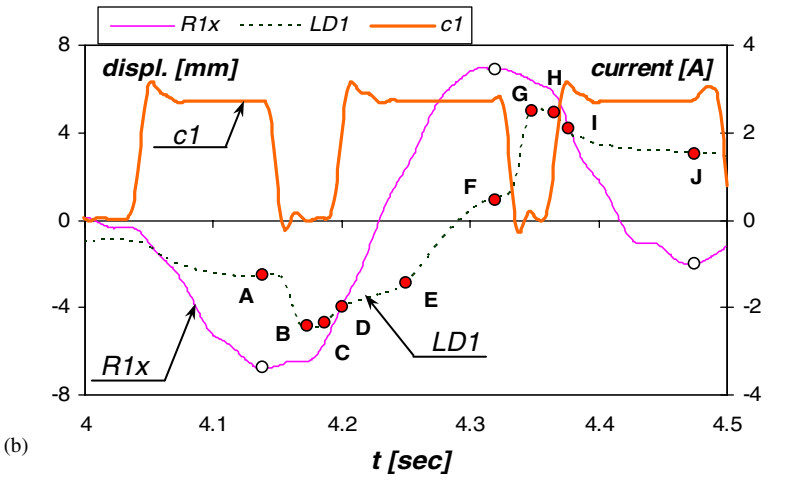

(b)

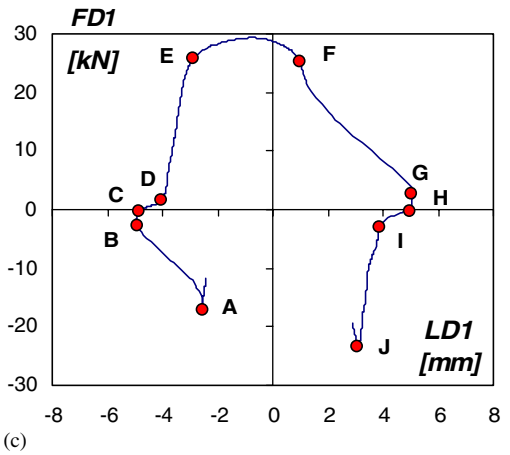

(c)

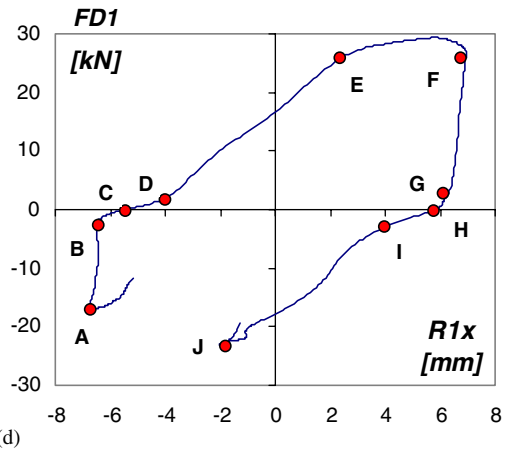

(d)

Figure 12. Detail of the operation of the SA system. Tolmezzo (SF = 1), SA_En.

D: at this point the slip phase of the control system is concluded (Figures 12c,d), the damper force begins its sharp increment (FD1, Figure 12a) and the accumulation (loading) phase of the brace starts;

D−E: the damper is in its ON operation, and the force is less than the 'frictional' threshold, i.e. the damper is in the stick phase, and its deformation is very small (LD1, Figure 12b); in this phase the damper stiffness, due to the connections, is detectable (Figure 12c). The significant frame deformation (Figure 12d) practically equals that of the brace, which is in its loading phase;

E: at this time the damper force equals the yielding force of the device, and the damper concludes its elastic behaviour (Figure 12c);

E−F: the damper, in ON operation, is in its 'plastic' phase, i.e. it shows large deformations without significant increments of the damper force and the viscous component of the post-elastic behaviour of the damper is clearly detectable (Figures 12a–c); the plasticization of the damper produces large displacements of the frame (R1x , Figures 12b,d), which remains in elastic stage: a significant amount of energy is dissipated by the damper in its hysteretic phase;

F: at this point the measured second-floor relative displacement reaches a relative maximum (R1x, Figure 12b), the sign of the corresponding relative velocity changes again (dX2, Figure 12a) and the device is deactivated. At this point, the current driving the MR dampers (c1, Figure 12b) starts to fall, and it again causes a sharp change in the force in the device (FD1, Figure 12a).

The last point F corresponds to the previous A point and a complete half-cycle of the SA system behaviour has been completed; in fact, the remaining steps, F–J, reproduce exactly the illustrated phases A–E.

6. MODELLING THE EXPERIMENTS

The analysis of the experimental evidence allows the formulation of a mathematical model of the MISS structure and of the passive and semi-active, ON–OFF, bracing system. The study of this mathematical model, of large importance for a complete understanding of the dynamical behaviour of the controlled structure and for predicting its response, will be illustrated and fully validated by comparing the results obtained in the numerical simulation of the tests with the experimental ones. Owing to practical absence of torsional response, the plane model of Figure 3 is considered in the following.

These numerical simulations have been performed using Simulink®, within a MATLAB® environment [25]; a fixed-step Runge-Kutta (ode4) solver has been used, with a minimum fixed step size (for the SA-controlled simulations) of 0.05 ms and all the numerical results have been sampled at 1000 Hz.

6.1. Unbraced MISS

In the plane model of the non-controlled MISS the bracings are not considered. For this model, which has four dynamic degrees of freedom only (X1–X4, Figure 3), a diagonal mass matrix and a full stiffness matrix have been derived on the basis of the actual experimental results in

the NC configuration:

$$\boldsymbol{M}_s = \begin{bmatrix} 5.679 & 0 & 0 & 0 \\ 0 & 5.679 & 0 & 0 \\ 0 & 0 & 5.679 & 0 \\ 0 & 0 & 0 & 5.679 \end{bmatrix} [\text{tons}] \tag{18}$$

$$\boldsymbol{K}_s = \begin{bmatrix} 110754.0 & -63347.4 & 20153.3 & -2772.9 \\ -63347.4 & 83565.0 & -55312.2 & 14074.6 \\ 20153.3 & -55312.2 & 66792.6 & -27785.7 \\ -2772.9 & 14074.6 & -27785.7 & 15951.1 \end{bmatrix} [\text{kN/m}] \tag{19}$$

With these mass and stiffness matrices, the modal frequencies are: $f_1 = 2.08$ Hz, $f_2 = 7.93$ Hz, $f_3 = 18.25$ Hz, $f_4 = 29.14$ Hz, and the corresponding modal shapes are shown in Figure 13. A proportional damping matrix, $\boldsymbol{C}_s = \alpha \boldsymbol{M}_s + \beta \boldsymbol{K}_s$, imposing a 2.5% damping factor on the first two modes, has been assumed ($\alpha = 0.5170\ s^{-1}$, $\beta = 0.7956 \times 10^{-3}$ s).

The first comparison between experimental and analytical results can be made on the transfer function obtained, in the experimental case, by means of the sine-sweep characterization tests. In Figure 14, the comparison between the experimental and analytical modula of the transfer functions from base to top (fourth-floor) absolute acceleration ($|H_{04}|$, Figure 14a) and from base to second-floor absolute acceleration ($|H_{02}|$, Figure 14b) are reported. In this figure the good agreement between experimental results and analytical model is shown. In particular, the first and third modal frequencies are well simulated (analytical: $f_{1,an} = 2.1$ Hz and $f_{3,an} = 18.3$ Hz, experimental: $f_{1,exp} = 2.2$ Hz and $f_{3,exp} = 18.7$ Hz) whereas the analytical frequency ($f_{2,an} = 7.9$ Hz) of the second mode is a bit lower than the experimental value ($f_{2,exp} = 8.7$ Hz). Also the modal dampings appear sufficiently approximated.

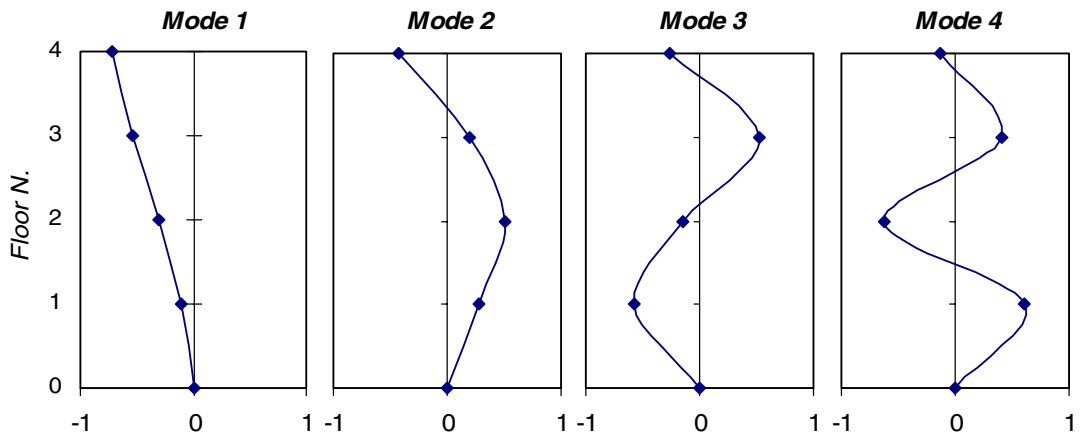

Figure 13. Modal shapes of the non-controlled MISS model.

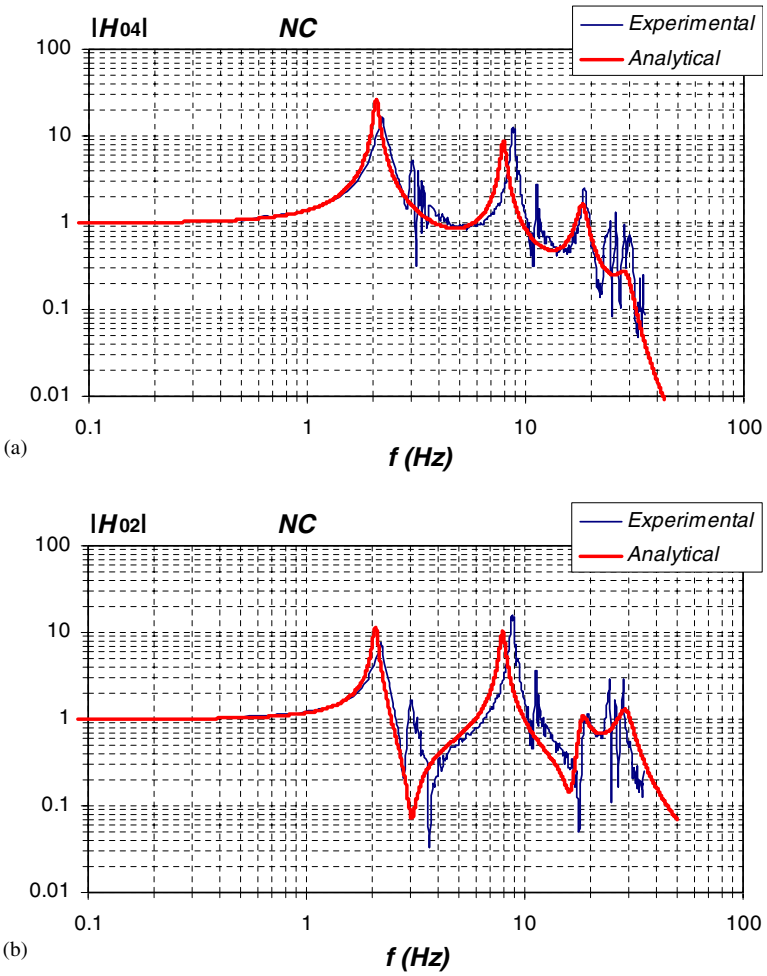

Figure 14. Transfer functions (a) $|H_{04}|$, (b) $|H_{02}|$. Experimental and analytical results, NC.

Very good accord between numerical and experimental results, both for displacements and fourth-floor absolute accelerations, are also confirmed in all the seismic tests, see e.g. Figure 15 where the second-floor displacement (X2) and fourth-floor (A4x,A8x) accelerations are reported.

6.2. *Model of the MR bracings: passive operation*

As described above, the bracings are composed by elastic steel columns connected to MISS by means of the MR dampers. By lumping the moving masses of the bracings, m_{b1} for the lower ones and m_{b2} for the upper ones, a plane model of the braced MISS may be considered in order to simulate its controlled transverse response (see Figure 3). In this model, the lower (1) or upper (2) stiffness $k_{b,i}$ represents the corresponding couple of braces, situated on the two sides of MISS (frame A and B). Considering the displacements of the bracing masses (X_5 and X_6), with respect

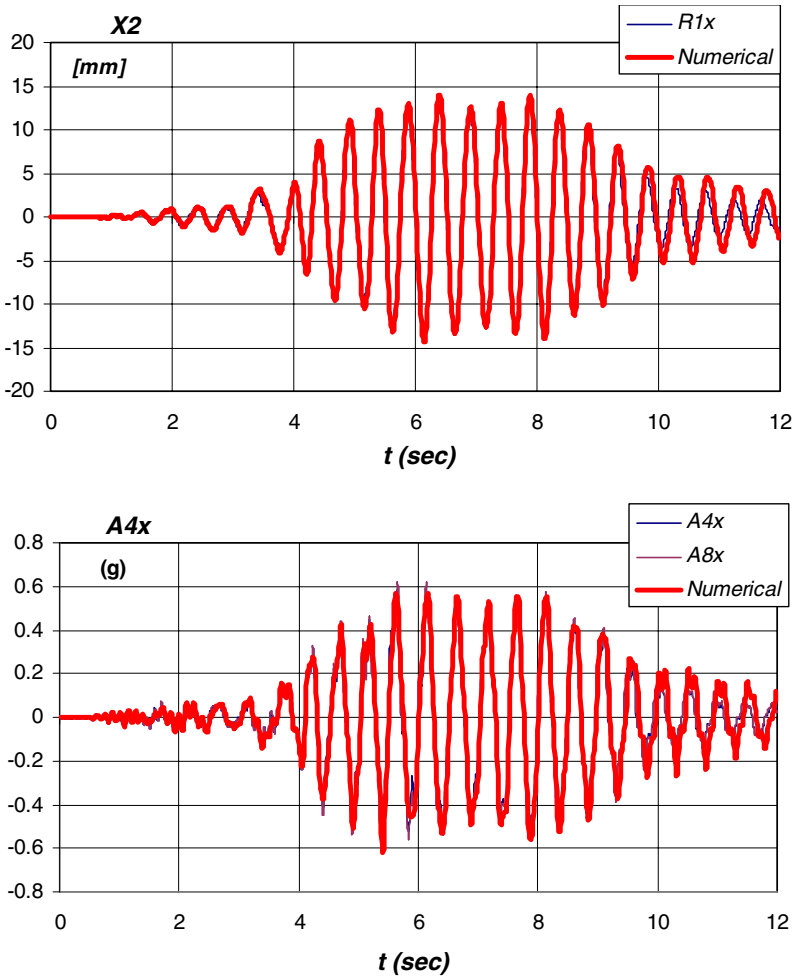

Figure 15. Experimental and numerical results, Tolmezzo (SF = 0.251), NC.

to the base as dynamical degrees of freedom, this model of the braced MISS has 6 (4 + 2) degrees of freedom in total.

As remarked in Section 2.3, the experimental tests on the MR dampers have shown the applicability of a nonlinear Bingham model (Equation 1) to the simulation of the constitutive laws of the MR dampers, tested before their installation on MISS. Furthermore, the observation of the actual behaviour of the MR dampers, installed on MISS, have already shown (Section 5.2) behaviour which may be ascribed to the assembling modality of the MR dampers to MISS and to the elastic braces and which should be considered in the analytical model. In particular, the Bingham model of the MR damper cannot predict the observed slip of the damper at zero force and the stiffness measured in the damper responses; moreover, the experimental tests have shown that a significant damping has been introduced in the braced structure, even if the MR threshold f_y is not reached and the frictional component is not activated; this fact may be ascribed to some non-modelled damping sources, located in the bracing assembly.

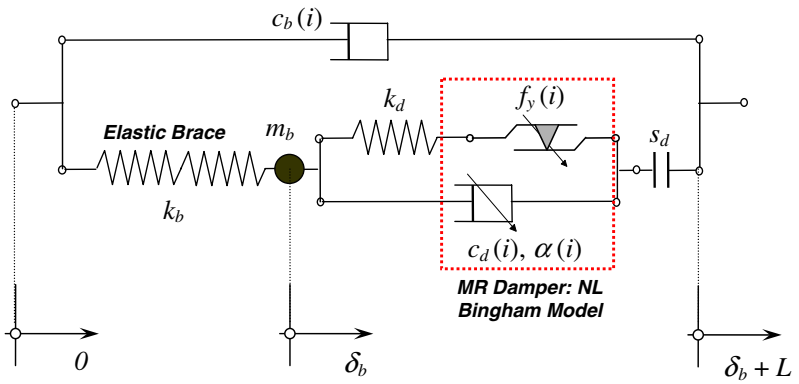

Figure 16. 'Improved' model of the MR bracing.

For these reasons an 'improved' rheological model for the whole MR bracing, which takes into account the above-mentioned characteristics of the actual response of the bracings installed on MISS, has been introduced (Figure 16). In this model, the MR device is again modelled by a Bingham rheological element, composed by the parallel assembling of a viscous and a frictional component (threshold f_y); in accordance with the results of the experimental tests on the MR dampers a nonlinear relationship between viscous damping force ($F_{v,d}$) and deformation velocity (U) is assumed:

$$F_{v,d}(U) = c_d |U|^{\alpha} \operatorname{sgn}(U) \tag{20}$$

The slip phenomena is modelled by a nonlinear gap element, which permits a displacement (up to the maximum opening s_d) at zero force. The elastic component, highlighted in the measured damper response, is modelled by an additional linear elastic element of stiffness k_d. This elastic component is in parallel with the viscous component of the MR damper, in this way the MR damper may also dissipate energy when the frictional component (with threshold f_y) is not activated.

The deformation of the MR damper L includes also the displacements of these gap and elastic elements, this is in accordance with the actual experimental measurements; the deformation of the elastic component (or the relative displacement of the brace mass m_b with respect the brace base) is called δ_b; the sum of δ_b and L represents the total deformation of the bracing.

Finally, an additional linear viscous damping element (coefficient c_b) has been introduced in order to take into account all the non-modelled dissipation sources due to the bracing assembly.

In conclusion, the proposed model of the MR bracing is characterized by the following eight mechanical parameters:

m_b: moving mass of the bracing;
k_b: stiffness of the elastic brace;
c_b: viscous damping associated with the whole bracing;
f_y: threshold of the frictional component of the MR damper Bingham model;
c_d: viscous coefficient of the MR damper Bingham model (Equation 20);
α: power of the velocity in the viscous component of the MR damper (Equation 20);
k_d: stiffness of the elastic component of the MR damper;
s_d: opening of the gap component of the MR damper.

Table II. Mechanical parameters of the 'improved' model for the MR bracings.

Parameters independent of current i			Parameters dependent on current i	
$m_{b1,2}$	0.17 tons		$i = 0$ A (OFF state)	$i = 2.5$ A (ON state)
k_{b1}	4400 kN/m	$c_{b1,2}$	0 kNs/m	25 kNs/m
k_{b2}	1755 kN/m	$f_{y1,2}$	0.9 kN	24.5 kN
$k_{d1,2}$	30000 kN/m	$c_{d1,2}$	5.5 kN(s/m)$^{0.9}$	18 kN(s/m)$^{0.53}$
s_{d1}	0.67 mm	$\alpha_{1,2}$	0.90	0.53
s_{d2}	0.33 mm			

The values of these mechanical parameters, characterizing the bracing and in general depending on the current i supplied to the MR dampers, have been obtained by fitting the available experimental result; referring to a single bracing, they are reported in Table II. In particular, regarding the mechanical parameters of the nonlinear Bingham model (f_y, c_d and α), the values obtained from the analysis of the experimental tests on the MR dampers (Equation 5) have been adopted [21].

Particular attention has been dedicated to the determination of the brace damping value c_b: in fact this damping is not directly correlated to a well-identified physical phenomenon, but includes all the non-modelled damping sources present in the bracing assembly. At 0 A current this damping has been set to 0, because the MR damper guarantees *per se* an adequate dissipation level. Instead, at 2.5 A current this additional damping is necessary, in particular for low-level inputs, because the MR damper, owing to the very high value of its internal stiffness k_d, shows a significant energy dissipation only if its frictional component is active (i.e. only if the damper force is larger than the MR threshold f_y). Therefore the chosen values of $c_{b1,2}$ have been selected by fitting, as well as possible, the experimental results, and in particular those obtained at low-level inputs.

The nonlinearity of the controlled MISS model does not permit the evaluation of analytical transfer functions; therefore, the characterization sweep-sine tests have been numerically simulated in order to compare the results obtained with the proposed analytical model with experimental values. The acceleration input used in these numerical simulations is a cosine sweep, with peak 0.01 g, and frequency linearly variable between 0 and 35 Hz with ratio 0.1 Hz/s.

Figures 17(a) and (b) report, respectively for 0 A current (OFF state) and 2.5 A current (ON state), the modulus of the transfer functions, from ground to top (fourth-floor, $|H_{04}|$) accelerations, experimentally obtained in the sweep-sine shaking table tests and in the numerical simulations.

The comparison shows a good accordance between numerical and experimental results, especially for the first and third modes, both in terms of frequency and damping. Regarding the second mode, for 2.5 A current, it appears significantly over-damped in the numerical simulations with respect to the experimental results; this is due to the bracing damping, necessary to the simulation of the non-modelled damping for low-level inputs.

Figures 18 and 19 report a selection of the results obtained by simulating the seismic shaking table tests, with MR dampers fed, respectively, at 0 and 2.5 A current, where it may be noted the good simulation of both the structural response time-histories (in terms of second-floor

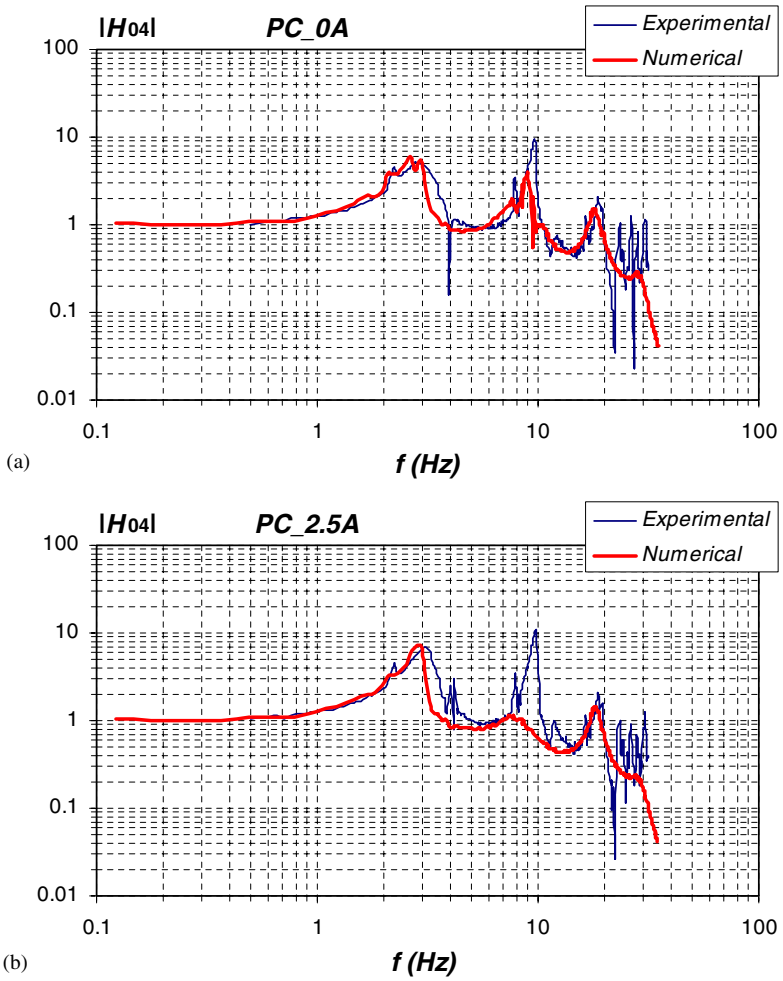

Figure 17. Transfer function $|H_{04}|$. Experimental and numerical results: (a) PC 0A; (b) PC 2.5 A.

displacements and top accelerations) and the force–displacement cycles of dampers and bracings. The very good accord between numerical and experimental results validates the analytical model of the passively controlled MISS, with dampers in OFF (0 A) and ON (2.5 A) state.

6.3. Model of the MR bracings: semi-active operation

In modelling the semi-active operation of the control system, the time variation of the MR damper mechanical parameters, in response to the ON–OFF current variations, has to be considered; this includes all the current-dependent parameters of the proposed model of the MR bracing.

In the present case of ON–OFF semi-active control, based on the algorithm of Equation 17, the MR devices are in the ON state for most of the time, and are deactivated only at particular

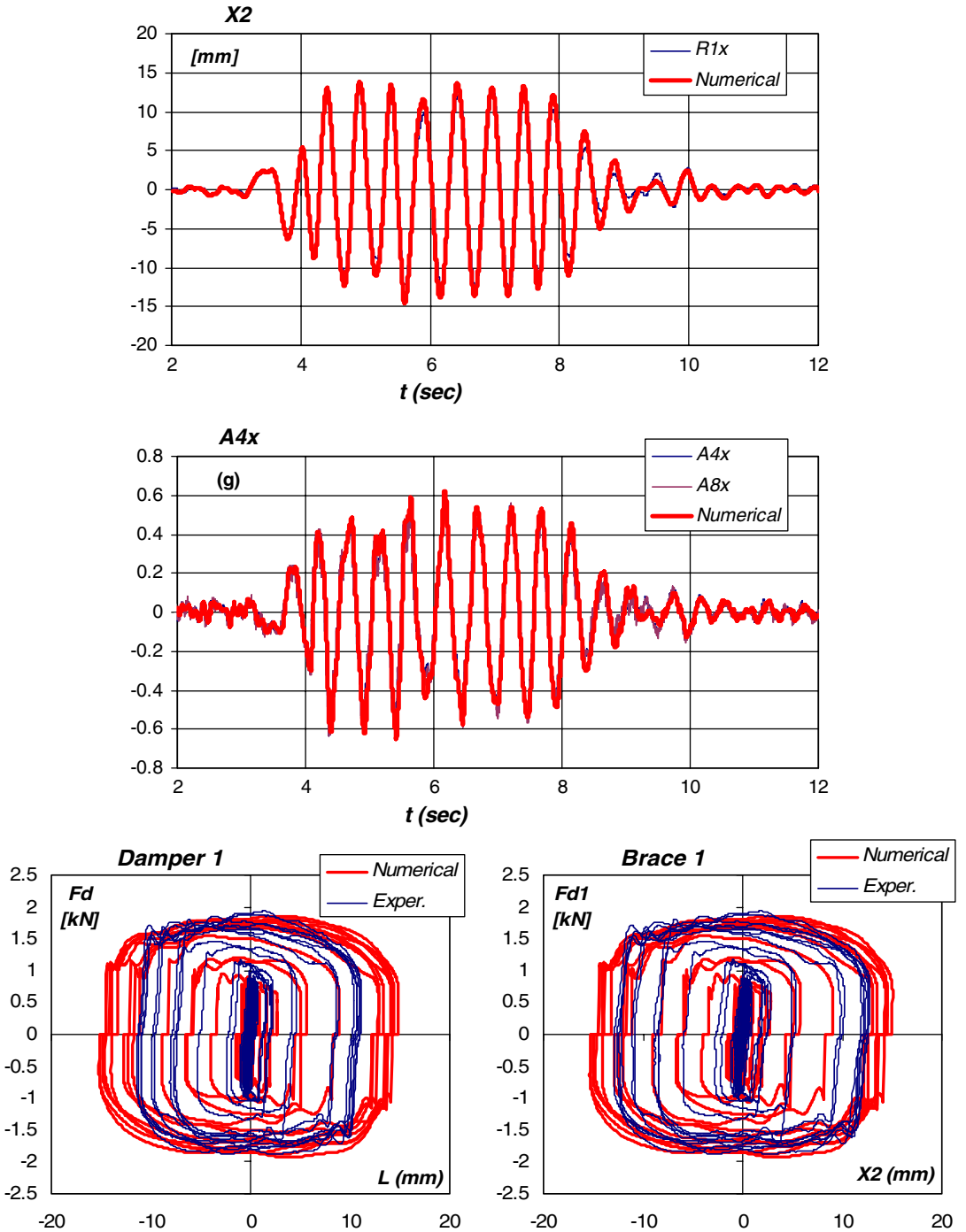

Figure 18. Experimental and numerical results, Tolmezzo (SF = 0.794), PC 0 A (OFF state).

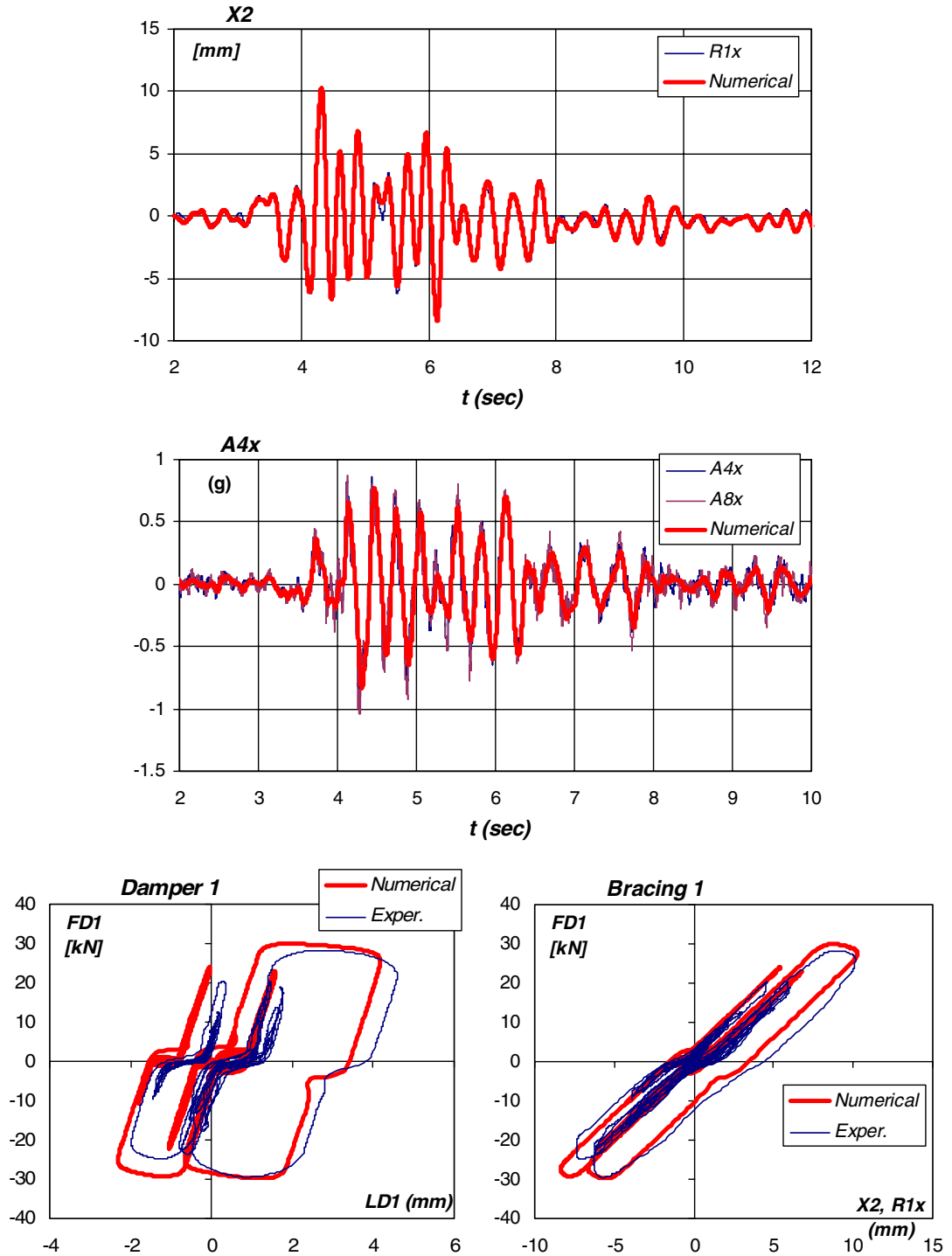

Figure 19. Experimental and numerical results, Tolmezzo (SF = 1), PC 2.5 A (ON state).

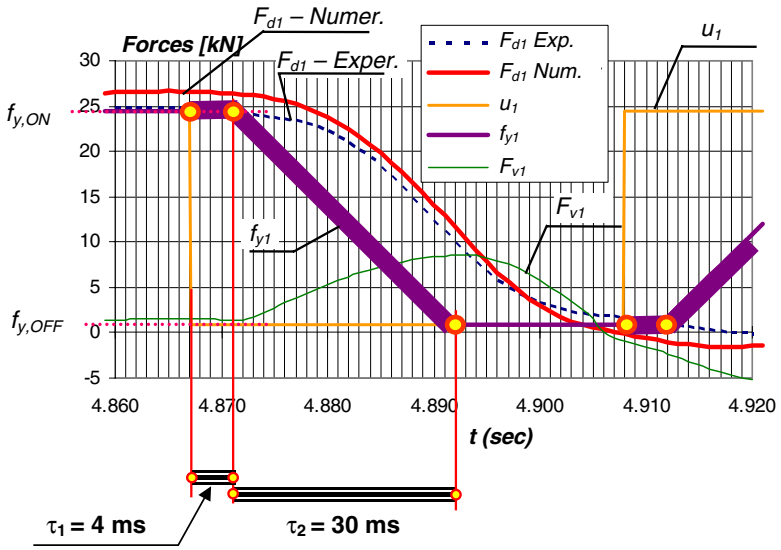

Figure 20. Model of the time variation of the MR damper force f_y.

time instants (selected by the control algorithm), in order to dissipate the recoverable energy accumulated in the elastic component of the bracings. For this motivation, a key point is modelling the deactivation phase of the MR dampers, in which their mechanical parameters go from the maximum values ($i = 2.5$ A, ON state) to the minimum values ($i = 0$ A, OFF state).

The assumed model of the time variation of the parameters in this deactivation process includes two phases. The first phase represents the delay between the realization of the deactivation analytical condition and the start of the actual time variation of the mechanical parameters; therefore, in this phase, the mechanical parameters stay at their maximum values. The time interval characterizing this phase will be called the *control delay* (τ_1). The second phase represents the time variation of the mechanical parameters from their maximum to their minimum values. This variation is modelled as linear in time, and it is completed in a characteristic time called the *damper dynamic time* (τ_2).

Starting from its maximum value, at the end of these two phases (i.e. after a time of $\tau_1 + \tau_2$ from the realization of the deactivation condition), the considered time-variant parameter assumes its minimal value. This model is illustrated, for the MR damper force f_y, in Figure 20, where F_d represents the total damper force (numerically evaluated and experimentally measured), u is the control signal obtained from the control algorithm (see Equation 17), f_y and F_v are, respectively, the numerically evaluated frictional and viscous components of the MR damper forces.

In the vast parametric study, it has been found that the *control delay* τ_1 may be set at 4 ms, whereas τ_2 depends on the mechanical parameter considered. In fact, for the threshold of the frictional component of the MR damper force (f_y), the characteristic time of the damper dynamic τ_2 may be set at 30 ms; these values are in accordance with those of Occhiuzzi *et al.* [21].

Instead, the parametric study has shown that the characteristic time of the deactivation process of the other current-dependent parameters (the parameters of the viscous component of

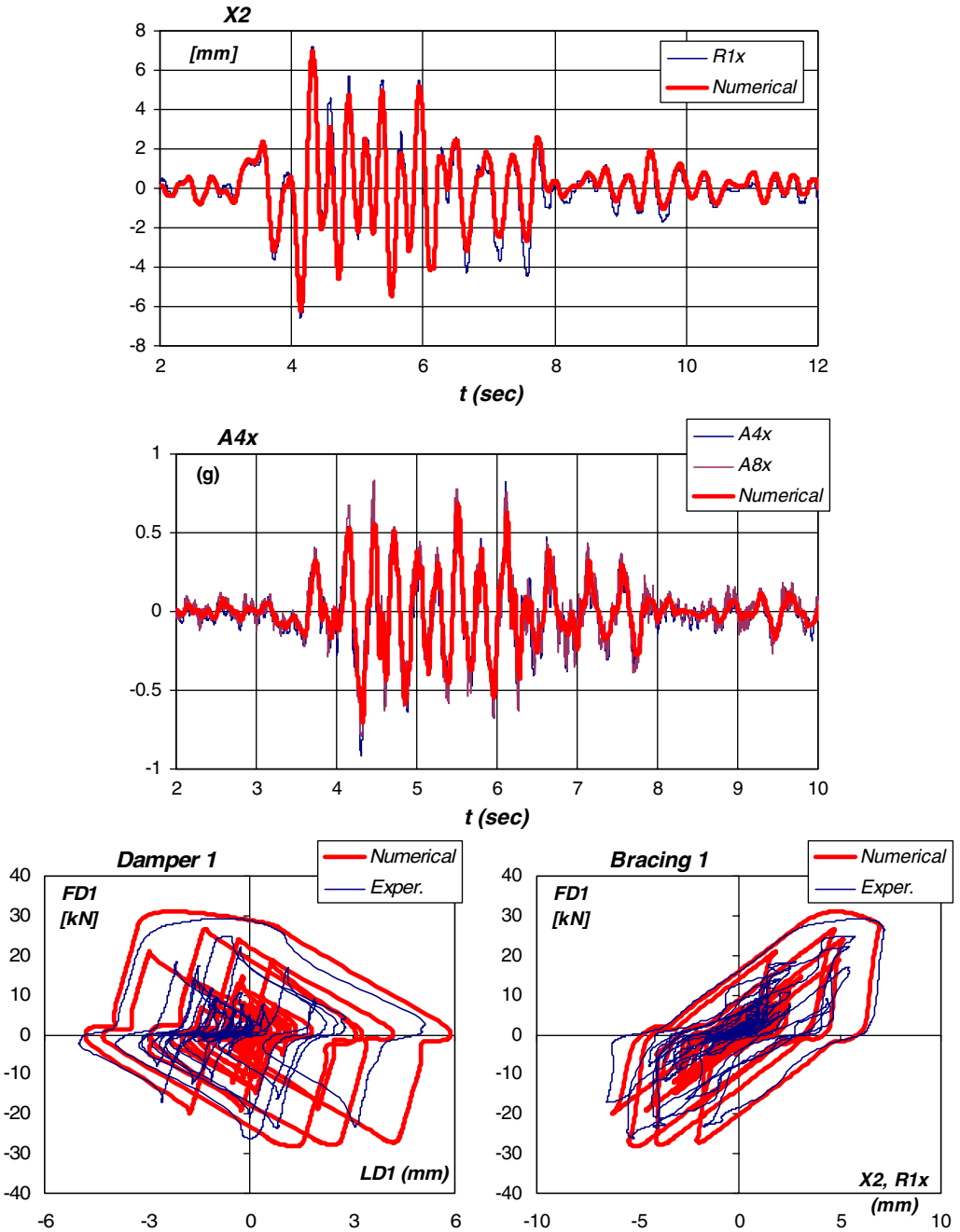

Figure 21. Experimental and numerical results, Tolmezzo (SF = 1), SA control.

the MR force, c_d and α, and the bracing damping c_b), is significantly larger with respect to the total time for which the damper is deactivated (Δt_{off}). Therefore, during all the deactivation process, these parameters stay practically at their maximum values, i.e. c_d, α and c_b remain constant throughout all the vibrations.

In the activation phase, a similar 'bilinear' model of the time variation of f_y is assumed (Figure 20), and the characteristic time intervals have the same values of the deactivation phase.

Figure 21 reports a simulation of a shaking table tests, where the good performance of this model of SA operation of the control system, both for response time-histories (second-floor displacements and top accelerations) and force–displacement cycles of dampers and bracings, are clearly shown.

7. CONCLUSIONS

In this paper, analyses of shaking table tests performed on a four-storey, large-scale, steel mock-up, equipped with a bracing system including magnetorheological (MR) dampers, operating both in passive and semi-active (SA) ON–OFF mode, have been presented.

A control algorithm, based on the minimization of a general instantaneous performance index, has been derived and a physical interpretation of the control process has been explained.

The critical overview of the experimental results obtained and the evaluation of the control performances, and in particular the evaluation of the response reductions obtained by using the SA-controlled MR dampers with respect to the corresponding passive system (devices always in the ON state), clearly shows the very good performance of the semi-active control system. In fact it is confirmed that using SA control not only reduces the maximum values of the response quantities considered (in particular in terms of displacements), but extends the improvements (for both displacements and accelerations) to the complete time-history.

This satisfactory behaviour of the semi-active control system has been obtained, even if some problems are detected, and explained, in the realization of the control process. In particular, large increments in the high-frequency component (at about 100 Hz) of the measured absolute accelerations, have been shown and explained. These disturbances, never highlighted in previous experimentations on SA control and strongly correlated with the device activations, confirm that SA control may increase the high-frequency component of the mass accelerations (as anticipated in previous theoretical work), making the comfort performance worse.

Furthermore, detailed analytical models, for the transverse motion of the steel mock-up, have been elaborated, for the uncontrolled (unbraced) and for the MR damper braced structure, both in passive and semi-active operation. These mathematical models have been set and fully validated by comparing the numerical results with the experimental ones, and permit a better understanding of the dynamical behaviour of the controlled structure and an adequate prediction of its response.

ACKNOWLEDGEMENTS

The research has been performed within WP7 of the SPACE project (Semi-active and PAssive Control of the dynamic behaviour of structures subjected to Earthquakes, wind and vibrations), funded by the European Commission (5th FP, 1998–2002), Contract EVG1-CT-1999-00016. The tests were performed 16–25 May 2002.

The authors would like to thank all the partners of the project:

- Maurer Söhne GmbH & Co. KG, in particular Dr R. Medeot and Mr J. Distl, for project coordination and manufacturing of MR devices;
- Bilfinger Berger Aktiengesellshaft, in particular Dr C. Seiler, for the help in the design of the control device;
- Thales Underwater Systems, in particular Dr G. Vanderborck and Mr G.P. Guido for the design and realization of the electronics of the control system;
- Kungl Tekniska Högskolan, for the study of MR fluids;
- ENEL.Hydro–ISMES, in particular Mrs G. Bergamo for the tests on the MR devices and the shaking table tests;
- ENEA, Ente per le Nuove Tecnologie, l'Energia e l'Ambiente, in particular Mr M. Forni, for making available the MISS mock-up and the design of its modifications;
- Università di Roma Tre, in particular Dr M. Spizzuoco, Dr A. Occhiuzzi and Dr F. Paolacci, for their continuous and fundamental collaboration in the preparation and execution of the tests,
- CESI;
- Tun Abdul Razak Research Center.

REFERENCES

1. Symans MD, Constantinou MC. Semi-active control systems for seismic protection of structures: a state-of-the-art review. *Engineering Structures* 1999; **21**(6):469–487.
2. Karnopp DC, Crosby MJ, Harwood RA. Vibration control using semi active force generation. *Journal of Engineering for Industry* (ASME) 1974; **96**(2):619–626.
3. Hrovat D, Barak P, Rabins M. Semi-active versus passive or active tuned mass dampers for structural control. *Journal of Engineering Mechanics* (ASCE) 1983; **109**(3):691–705.
4. Renzi E. *Semi-active control of Structural Vibrations*: *Theory and Applications*. PhD Dissertation, Department of Structural and Geotechnical Engineering, University of Rome 'La Sapienza', December 2001 (in Italian).
5. Kurata N, Kobori T, Takahashi M, Niwa N, Kurino H. Shaking table experiment of active variable damping systems. *Proceedings of the 1st World Conference on Structural Control*, Los Angeles, 1994; **2**:TP2/108–117.
6. Symans MD, Constantinou MC. Seismic testing of a building structure with semi-active fluid damper control system. *Earthquake Engineering and Structural Dynamics* 1997; **26**(7):759–777.
7. Symans MD, Madden GJ, Wongprasert N. Experimental study of an adaptive base isolation system for buildings. *Proceedings of the 12th World Conference on Earthquake Engineering* 12WCEE, Auckland, 30 January–4 February 2000, paper 1965. CD-ROM.
8. Lee GC, Liang Z, Tong M. Development of a semi-active structural control system. *Research Progress and Accomplishments 1997–1999*. Multidisciplinary Center for Earthquake Engineering Research MCEER, SUNY at Buffalo, NY (USA), July 1999. http://mceer.buffalo.edu/publications/resaccom/9799/default.asp [19 March 2003].
9. Dyke SJ, Spencer BF, Sain MK, Carlson JD. Experimental verification of semi-active structural control strategies using acceleration feedback. *Proceedings of the 3rd International Conference on Motion and Vibration Control*, Chiba, 1–6 September 1996, **3**:291–296.
10. Yi F, Dyke SJ, Caicedo JM. Experimental verification of multi-input seismic control strategies for smart dampers. *Journal of Engineering Mechanics* (ASCE) 2001; **127**(11):1152–1164.
11. Ruangrassamee A, Kawashima K. Semi-active control of bridges with use of magnetorheological damper. *Proceedings of the 12th European Conference on Earthquake Engineering*, London, September 2002, paper 171. CD-ROM.
12. Lin PY, Chung LL, Loh CH, Cheng CP, Roschke PN, Chang CC. Experimental study of seismic protection for structures using MR dampers. *Proceedings of the 12th European Conference on Earthquake Engineering*, London, September 2002, paper 249. CD-ROM.
13. Serino G, Occhiuzzi A, Georgakis CT. Experimental study and perspectives of semi-active oleodynamic devices for seismic protection of structures. *Experimental investigations of semi-active and passive systems for seismic risk mitigation*, CAFEEL-ECOEST2/ICONS Report 7, Part 1, June 2001, Franchioni G (ed.), Laboratòrio Nacional de Egenharia Civil, Lisboa, Portugal.
14. Kobori T, Takahashi M, Nasu T, Niwa N. Seismic response controlled structure with active variable stiffness systems. *Earthquake Engineering and Structural Dynamics* 1993; **22**:925–941.
15. Patten WN, Sun J, Li G, Kuehn J, Song G. Field test of an intelligent stiffener for bridges at the I-35 Walnut Creek Bridge. *Earthquake Engineering and Structural Dynamics* 1999; **28**(2):109–126.

16. Kurata N, Kobori T, Takahashi M, Niwa N, Midorikawa H. Actual seismic response controlled building with semi-active damper system. *Earthquake Engineering and Structural Dynamics* 1999; **28**(11):1427–1447.
17. Yoshida K, Fujio T. Semi-active base isolation control of a building using variable damper oil damper. *Proceedings of the 3rd International Workshop on Structural Control*, Paris, 6–8 July 2000; 567–575.
18. Ciampi V, De Angelis M, Renzi E. Optimal semi active and passive control of the seismic response of coupled frame-bracing systems. *Proceedings of the 12th World Conference on Earthquake Engineering* 12WCEE, Auckland, 30 January–4 February 2000, paper 2288. CD-ROM.
19. Renzi E, De Angelis M, Ciampi V. Optimal semi-active control of MDOF structures. *Proceedings of the 5th European Conference on Structural Dynamics*, Munich, 2–5 September 2002; **2**:991–996.
20. Serino G, Spizzuoco M. About the design of passive and semi-active MR dampers for seismic protection of buildings. *Proceedings of the 12th European Conference on Earthquake Engineering*, London, September 2002, paper 709. CD-ROM.
21. Occhiuzzi A, Spizzuoco M, Serino G. Experimental analysis of magnetorheological dampers for structural control. *Smart Materials and Structures*.
22. Yang JN, Akbarpour A, Ghaemmaghami P. New optimal control algorithms for structural control. *Journal of Engineering Mechanics* (ASCE) 1987; **113**(9):1369–1387.
23. Inaudi JA, Hayen JC. Research on variable-structure systems in the US. *Proceedings of the International Post-Smirt Conference and Seminar on Seismic Isolation, Passive Energy Dissipation and Control of Structures*, Santiago, Chile, August 1995; 591–622.
24. National Instruments. *LabVIEW™ User Manual*. National Instruments Corporation, Austin, Texas USA, 2000.
25. MatWorks. Simulink® Dynamic System Simulation for Matlab® Using Simulink. The MatWorks Incorporated, Natick Massachusetts, USA, 1999.

